

Czech Technical University in Prague  
Faculty of Nuclear Sciences and Physical Engineering  
Department of Nuclear Chemistry

## Continuous extraction and detection of homologues of transactinides



Bachelor Thesis

Thesis Author: Lucie Šifnerová  
Supervisor: Ing. Pavel Bartl, Ph.D.  
Consultant: prof. Ing. Jan John, CSc.

2023

## I. OSOBNÍ A STUDIJNÍ ÚDAJE

Příjmení: Šifnerová Jméno: Lucie Osobní číslo: 502415  
Fakulta/ústav: Fakulta jaderná a fyzikálně inženýrská  
Zadávající katedra/ústav: Katedra jaderné chemie  
Studijní program: Jaderná chemie

## II. ÚDAJE K BAKALÁŘSKÉ PRÁCI

Název bakalářské práce:

**Kontinuální extrakce a detekce homologů transaktinoidů**

Název bakalářské práce anglicky:

**Continuous extraction and detection of homologues of transactinides**

Pokyny pro vypracování:

1. Vypracování přehledu o současném stavu problematiky ve světě. Důraz bude kladen na rešerši principů funkce průtokových radiometrických detektorů pro malé objemy kapalin.
2. Vytipování vhodných kontinuálních detekčních systémů pro detekci homologů transaktinoidů studovaných na KJCH.
3. Testování vytipovaných detekčních systémů.

Seznam doporučené literatury:

- [1] Knoll, G. F. Radiation Detection and Measurement. 4th edition, John Wiley & Sons Inc, 2010. ISBN 978-0-470-13148-0.
- [2] Schädel, M., Shaughnessy, D., eds. The Chemistry of Superheavy Elements. Second edition, Springer-Verlag Berlin Heidelberg, 2014. ISBN 978-3-642-37465-4.
- [3] Firemní literatura výrobců a dodavatelů radiometrických detektorů pro HPLC
- [4] Firemní literatura výrobců a dodavatelů radiometrických detektorů pro FIA (Flow Injection analysis)

Jméno a pracoviště vedoucí(ho) bakalářské práce:

**Ing. Pavel Bartl, Ph.D. katedra jaderné chemie FJFI**

Jméno a pracoviště druhého(ho) vedoucí(ho) nebo konzultanta(ky) bakalářské práce:


**prof. Ing. Jan John, CSc. katedra jaderné chemie FJFI**

Datum zadání bakalářské práce: **20.10.2022**

Termín odevzdání bakalářské práce: **02.08.2023**

Platnost zadání bakalářské práce: **20.10.2024**

  
Ing. Pavel Bartl, Ph.D.  
podpis vedoucí(ho) práce

  
podpis vedoucí(ho) ústavu/katedry

  
doc. Ing. Václav Čubá, Ph.D.  
podpis děkana(ky)

## III. PŘEVZETÍ ZADÁNÍ

Studentka bere na vědomí, že je povinna vypracovat bakalářskou práci samostatně, bez cizí pomoci, s výjimkou poskytnutých konzultací. Seznam použité literatury, jiných pramenů a jmen konzultantů je třeba uvést v bakalářské práci.

**29-10-2022**

Datum převzetí zadání



  
Podpis studentky

## Acknowledgements

I would like to express my deepest gratitude to my supervisor Ing. Pavel Bartl, Ph.D for his continuous guidance, support, and valuable insights during writing this thesis. Ing. Pavel Bartl, Ph.D patiently shared his knowledge and expertise with me and also provided me with valuable resources and access to facilities.

Declaration

I hereby declare that I have written the bachelor thesis solely by myself under the professional supervision of Ing. Pavel Bartl, Ph.D. and that no other sources, other than listed in the references, have been used.

In Prague on ..... 2. 8. 2023 .....



.....

Lucie Šifnerová

Title: Continuous extraction and detection of homologues of transactinides

Author: Lucie Šifnerová

Branch: Nuclear Chemistry

Type of thesis: Bachelor Thesis

Supervisor: Ing. Pavel Bartl, Ph.D.

CTU in Prague, FNSPE, Department of Nuclear Chemistry

Consultant: prof. Ing. Jan John, CSc.

CTU in Prague, FNSPE, Department of Nuclear Chemistry

Abstract: Transactinides are artificial elements that are formed through nuclear reactions with usually very low yields. Due to their short half-lives, the study of their behaviour is challenging not only from an experimental, but also from a financial point of view. Therefore, preliminary experiments with their homologues, which ensure obtaining more accurate estimates of their behaviour, are often carried out before the actual investigation of transactinides.

The theoretical part of this thesis describes the preparation of transactinides and their homologues, especially thallium homologues, which was the main subject of the experiments. Furthermore, experimental techniques for investigating transactinides in the liquid phase are described, with an emphasis on individual components and their various forms used in the world. The thesis also deals with the efficiency of the transport of the investigated isotopes from the source (accelerator) to the laboratory and various methods of their detection.

The aim of the experimental part of this thesis is to ensure the most efficient and fastest possible transport of radionuclides from the cyclotron-irradiated target to the laboratory, more precisely into the impactor part of the particle-into-liquid sampler (PILS), where the radionuclides are collected and dissolved. The transport times in and out of the impactor part of the PILS during the irradiation are investigated. These experiments aim to improve and optimize processes that contribute to increasing the efficiency and reliability of the study of transactinides in the liquid phase at the CTU in Prague.

Keywords: Transactinides, homologues, transport time,  $^{195m}\text{Tl}$ , PILS

Název práce: Kontinuální extrakce a detekce homologů transaktinoidů

Autor: Lucie Šifnerová

Obor: Jaderná chemie

Druh práce: Bakalářská práce

Vedoucí práce: Ing. Pavel Bartl, Ph.D.  
ČVUT v Praze, FJFI, Katedra jaderné chemie

Konzultant: prof. Ing. Jan John, CSc.  
ČVUT v Praze, FJFI, Katedra jaderné chemie

Abstrakt: Transaktinoidy jsou umělé prvky, které vznikají prostřednictvím jaderných reakcí, které mají obvykle velmi nízké výtěžky. Vzhledem k jejich krátkým poločasům přeměny je studium jejich chování náročné nejen z experimentálního, ale i finančního hlediska. Proto se před samotným zkoumáním transaktinoidů provádějí experimenty s jejich chemickými homology za účelem získání přesnějších odhadů jejich chování.

V teoretické části bakalářské práce je popsána příprava transaktinoidů i jejich homologů, zejména pak homologů thalia, které bylo použito v experimentální části práce. Dále jsou popsány experimentální techniky a aparatury pro zkoumání transaktinoidů v kapalně fázi s důrazem na jednotlivé komponenty a jejich různé variace používané ve světě. Práce se zabývá efektivitou transportu zkoumaných izotopů od zdroje (urychlovače) do laboratoře a různými způsoby jejich detekce.

Cílem experimentální části této bakalářské práce je zajištění co nejefektivnějšího a nejrychlejšího transportu od ozařovaného terče do laboratoře, konkrétně do dopadové části zařízení PILS (z angl. Particle-into-liquid sampler), kde dochází ke sběru a rozpouštění připravených radionuklidů. Zkoumá se rychlost transportu do dopadové části zařízení PILS během ozařování a rychlost transportu ze zařízení PILS ven během vypnutí svazku. Tyto experimenty mají za cíl zlepšit a optimalizovat procesy, které přispívají ke zvýšení efektivity a spolehlivosti studia transaktinoidů v kapalně fázi na ČVUT v Praze.

Klíčová slova: Transaktinoidy, homology, rychlost transportu,  $^{195m}\text{Tl}$ , PILS

## Table of Contents

<b>Introduction .....</b>	<b>9</b>
<b>1 Transactinides .....</b>	<b>10</b>
1.1 Properties of transactinides.....	10
1.2 Synthesis of transactinides .....	11
<b>2 Homologues of transactinides .....</b>	<b>12</b>
2.1 Thallium as a homologue of nihonium .....	12
2.2 Preparation of thallium isotopes .....	12
<b>3 Experimental techniques and systems for aqueous chemistry .....</b>	<b>14</b>
<b>3.1 Kinematic pre-separators .....</b>	<b>14</b>
3.1.1 Berkeley gas-filled separator (BGS).....	14
3.1.2 Transactinide separator and chemistry apparatus TASCA .....	14
3.1.3 Dubna gas-filled recoil separator (DGFRS) .....	15
3.1.4 Gas-filled recoil ion separator (GARIS).....	16
<b>3.2 Gas-jet transport (GJT) system.....</b>	<b>18</b>
3.2.1 Aerosol GJT system .....	18
3.2.2 TRIGA-SPEC facility.....	19
3.2.3 SINQ (Swiss spallation neutron source) facility.....	20
<b>3.3 Dissolution techniques .....</b>	<b>21</b>
3.3.1 Preconcentration and washing out.....	21
3.3.2 Stationary mixer and degasser centrifuge .....	23
3.3.3 Membrane degasser (MDG).....	23
3.3.4 Particles-into-liquid sampler (PILS) .....	24
<b>4 Continuous detection techniques .....</b>	<b>24</b>
<b>4.1 Detection of transactinides.....</b>	<b>24</b>
4.1.1 Alpha spectrometry .....	24
4.1.2 Liquid scintillation .....	25
<b>4.2 Continuous gamma detection – residence time distribution .....</b>	<b>25</b>
4.2.1 Residence Time Distribution (RTD) .....	25
4.2.2 Continuous gamma detection.....	27
<b>5 Experimental .....</b>	<b>28</b>
<b>5.1 Cyclotron U-120M .....</b>	<b>28</b>
<b>5.2 Modular robotic gas-jet target system (MARGE).....</b>	<b>28</b>
<b>5.3 Recoil transfer chamber and gas-jet transport system .....</b>	<b>28</b>
<b>5.4 Gas mixing chambers.....</b>	<b>29</b>
5.4.1 Glass mixing chamber .....	29
5.4.2 Gas mixer .....	30
<b>5.5 Particles-into-liquid sampler (PILS) .....</b>	<b>30</b>

5.6	Detection .....	31
5.7	Statistics.....	32
<b>6</b>	<b><i>Results and discussion</i></b> .....	<b>33</b>
6.1	Data pretreatment .....	33
6.2	Comparison of flow rates.....	33
	<b><i>Conclusion</i></b> .....	<b>36</b>
<b>7</b>	<b><i>References</i></b> .....	<b>37</b>



## Introduction

Since the transactinides lie at the edge of the current periodic table of elements, they offer an interesting opportunity for study, as humans love to push the limits and explore the unknown. The fact that humans were able to synthesize completely new elements has motivated many to consider the possibility that there is no "end" to the periodic table. However, these are probably just fantasies; nevertheless, the researchers can strive to do their best and stretch the "end" towards its limits. Even if an unlimited number of new elements cannot be produced artificially, understanding, and discovering the properties of the transactinides may play a vital role in development of science, as such understanding may lead to other ground-breaking discoveries.

By researching various extraction and detection methods, researchers are getting closer to obtaining more valuable information about the transactinides. Research focused on improving the current methods and finding the optimal parameters for the most efficient operations of the devices is crucial on this path to understanding.

The transactinides provide challenges not just because they are notoriously known for their extremely short half-lives, but also because their production is financially challenging, and their production rates are very low (atoms per day to atoms per week).

This thesis builds on previous research conducted at the Department of Nuclear Chemistry, FNSPE, CTU, with the focus on the research of various methods of detection and extraction used in the field of transactinide chemistry all around the world. In addition to thorough research of the methods, the objective is to further optimize the current liquid chemistry apparatus developed at the CTU, to achieve better results, and pave the way for future research.

# 1 Transactinides

Transactinides, also referred to as superheavy elements (SHEs), are elements with atomic number 104 and higher (Hofmann *et al.*, 2018). They belong to groups 4 – 18 of the 7<sup>th</sup> period of the periodic table of elements (PTE), which makes them a rather unusual “group” in terms of the PTE. Since they do not belong to the same group of the PTE, their properties are supposed to vary one from another. Similarity, which connects all the transactinides, and makes them a group in a way, is their unusual physical-chemical properties, resulting in their low-yield and complex production processes and high instability. Transactinides are produced artificially, they do not occur in the nature normally.

While the first transactinides were discovered in 1960s, the latest discovered elements were acknowledged by IUPAC at the end of 2015 when the approval was announced. Newly approved elements were 113, 115, 117 and 118 with their names announced in 2016: nihonium, moscovium, tennessine and oganesson respectively (Karol *et al.*, 2016).

104 267.1... <b>Rf</b> Rutherfordium Transition Metal	105 268.1... <b>Db</b> Dubnium Transition Metal	106 269.1... <b>Sg</b> Seaborgium Transition Metal	107 270.1... <b>Bh</b> Bohrium Transition Metal	108 269.1... <b>Hs</b> Hassium Transition Metal	109 277.1... <b>Mt</b> Meitnerium Transition Metal	110 282.1... <b>Ds</b> Darmstadtium Transition Metal	111 282.1... <b>Rg</b> Roentgenium Transition Metal	112 286.1... <b>Cn</b> Copernicium Transition Metal	113 286.1... <b>Nh</b> Nihonium Post-Transition M...	114 290.1... <b>Fl</b> Flerovium Post-Transition M...	115 290.1... <b>Mc</b> Moscovium Post-Transition M...	116 293.2... <b>Lv</b> Livermorium Post-Transition M...	117 294.2... <b>Ts</b> Tennessine Halogen	118 295.2... <b>Og</b> Oganesson Noble Gas
--	--	---	--	--	---	---	--	--	---	--	--	--	--	---

Figure 1: Depiction of transactinide elements in the PTE. Adopted from PubChem.

## 1.1 Properties of transactinides

Learning the properties of transactinides is very demanding both from the theoretical and experimental point of view. Transactinides are produced in extremely small amounts ranging usually from one atom per day to one atom per week. Additionally, the instability of known isotopes of transactinides, with usual half-lives ranging from tens of milliseconds to tens of seconds, is further hindering the research of their properties (Terranova, Tavares, 2022).

According to the periodic law, similar properties within the respective groups of transactinide elements should be expected. However, due to increasing relativistic effects, deviations in periodicity of the properties are predicted. The Coulomb field of the nucleus increases with its growing charge and mass, which greatly accelerates nearby electrons in the shell making them relativistic particles. The atomic *d* and *f* orbitals can be deformed by these effects, and abnormal electron configurations may occur, leading to oxidation states different from the rest of the elements in the group. (Schwerdtfeger, Smits, Pyykkö, 2020) The significance of the relativistic effects grows with the increase in atomic number.

Furthermore, with increasing atomic number, *Z*, the stability decreases; that is a general trend for currently known isotopes of transactinides as they are still far from the island of stability (IoS) (Thompson., Tsang, 1972). IoS is predicted area on the *N/Z* map where more stable isotopes are expected to be found. This increased stability is tied with “magic numbers”. Elements with magic numbers, which are certain numbers of protons and neutrons, show higher stability due to the fully occupied nuclear shells. Known magic numbers, as well as the predicted ones (highlighted in green), are shown in table 1.

Table 1: Magic numbers for atomic numbers and neutron numbers. Predicted magic numbers are highlighted in green.

Z	2	8	20	28	50	82	120 or 126	
N	2	8	20	28	50	82	126	184

Doubly magic nuclei, i.e., nuclei with the number of protons as well as neutrons corresponding to the magic numbers, are the most stable ones. Therefore, it is expected that the peak of IoS is present around the element with the next doubly magic numbers. This nucleus is yet to be synthesized. Granted the increased stability, it would be possible to study superheavy elements on a deeper scale, once isotopes from the vicinity of the IoS are available (Oganessian., Rykaczewski, 2015).

## 1.2 Synthesis of transactinides

Transactinides are produced through fusions of accelerated heavy ions with target nuclei. The fusion, therefore, a creation of new nucleus, can be achieved if the projectile has sufficient energy to overcome the Coulomb barrier between the nuclei. However, the probability of fusion of the target and beam nuclei leading to the production of a transactinide is extremely low and it is more likely that quasi-fission or fission will occur as shown in figure 2, where the evaporation residue represents the product of interest (Hagino, 2019). To obtain a new nucleus of required element via full fusion reaction, the sum of protons in the projectile and the target must be the equal to the Z of the desired product (Terranova, Tavares, 2022).

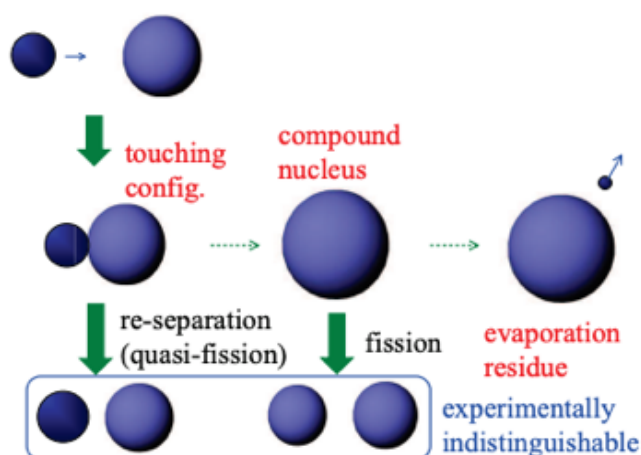


Figure 2: Schematic illustration of heavy ion fusion leading to creation of superheavy nuclei. Adopted from (Hagino, 2018).

For preparation of transactinides, projectile particles are accelerated in a cyclotron or other type of accelerator. Accelerated particles are directed to the target foil containing target nuclei. One of the possible reaction outcomes, as mentioned above, is a compound nucleus. The compound nucleus is highly excited, and it undergoes a process of evaporation of neutrons, forming more stable EVR. However, the resulting EVR is multiply charged and still has rather high energy. Naturally, such atom needs to stabilize itself (lose energy and gain electrons), which is achieved due to collisions with a gas environment that is placed directly behind the target (either within a gas-filled separator or a gas-jet transport system; see chapter 3 for more details).

## 2 Homologues of transactinides

As mentioned in section 1.2, the means of production of transactinides are difficult and so far, only their short-lived isotopes had been found. For this reason, homologues of transactinides, elements occupying the same group in the PTE, and thus, possessing similar properties according to the periodic law, can be used to develop the most efficient separation methods, which can be transferred onto the transactinide research and used for learning the properties of real transactinides (Terranova, Tavares, 2022). Due to the relativistic effects, mentioned in section 1.1, the properties of transactinides may differ from their respective homologues and may be, for example, closer to the homologues of the neighbouring groups. For this reason, even under the same experimental conditions, results obtained for the homologues and transactinides themselves may not follow the same trend; hence, it is important to consider comparison of results with trends of surrounding (groups of) elements as well. Due to the nature of the experimental part of this work, homologues of the group 13 will be discussed into more detail.

### 2.1 Thallium as a homologue of nihonium

Thallium (Tl) is a homologue of nihonium (Nh) and together with boron (B), aluminium (Al), gallium (Ga) and indium (In) form the 13th group of the PTE. Except for boron, all the other elements in the group 13 are metals. For this reason, the behaviour of boron highly differs from the rest of the group. For the comparison of properties with the respective transactinide, usually the heaviest homologues are relevant, i.e., In and Tl in this case. It is expected that nihonium will have similar atomic radius to thallium despite being in higher period. This is caused by the contractions of orbitals  $7s$  and  $7p_{1/2}$ . All metallic elements in the group 13 have low electrical resistivity and low melting point. Thallium's melting point specifically is  $303,5\text{ }^{\circ}\text{C}$ . Thallium is slightly different in reactivity compared to other elements occupying the group 13. Thallium's most common oxidation states are +1 and +3, which is different from its lighter homologue In, that forms only stable +1 state (In-like behaviour is also predicted for Nh). However, a reduction from the +3 state to the +1 state is spontaneous under normal conditions. Therefore, +1 oxidation state is more common for thallium. Elemental thallium is prone to tarnishing when exposed to humid environment and forms TlOH, a strong base. Thallium also forms  $\text{TlF}_3$ , but it is less stable than trihalides of other group 13 members. It quickly hydrolyses to  $\text{Tl}(\text{OH})_3$  and HF.  $\text{TlCl}_3$ ,  $\text{TlBr}_3$  and  $\text{TlI}_3$  can be also formed. The +1-state halides of thallium are more stable than the +3-state ones and are poorly soluble in water (Greenwood, Earnshaw, 1997).

### 2.2 Preparation of thallium isotopes

For the best simulation of short-lived transactinides, a short-lived isotope of a homologue should be used in the experiments. Such short-lived isotopes of thallium can be prepared by reaction of accelerated  $^3\text{He}$  and  $^{197}\text{Au}$ , which is monoisotopic, so the reaction is well defined (Bartl, 2022). The half-lives, radioactive decay modes and distinctive gamma lines are showed in table 2 for chosen isotopes of thallium.

Table 2: Summary of reactions leading to selected thallium isotopes<sup>1</sup>

<b>Reaction</b>	<b><math>T_{1/2}</math> [s]</b>	<b>Radioactive decay mode</b>	<b><math>E_{\gamma}</math> [keV]<sup>2</sup></b>
$^{197}\text{Au}(\ ^3\text{He}, 4n)^{196}\text{Tl}$	6624	100 % $\beta^+$	634.90, 964.77, 1495.91, 1553.77
$^{197}\text{Au}(\ ^3\text{He}, 4n)^{196m}\text{Tl}$	5076	96.2 % $\beta^+$ , 3.8 % IT	120.35, 301.7, 504.12, 634.90, 723.6
$^{197}\text{Au}(\ ^3\text{He}, 5n)^{195}\text{Tl}$	4176	100 % $\beta^+$	1347.5, 1512.7
$^{197}\text{Au}(\ ^3\text{He}, 5n)^{195m}\text{Tl}$	3.6	100 % IT	383.52
$^{197}\text{Au}(\ ^3\text{He}, 6n)^{194}\text{Tl}$	1980	100 % $\beta^+$	634.9, 1073.9
$^{197}\text{Au}(\ ^3\text{He}, 6n)^{194m}\text{Tl}$	1968	100 % $\beta^+$	228.5, 634.9, 650.1, 735.5

The emphasis, when it comes to simulating transactinide-like conditions, can be put on the 3.6-second isotope  $^{195m}\text{Tl}$ . Due to the very low half-life, it can be exploited for optimizing the on-line detection process of a fast chemical apparatus or for exploring dynamics of its subprocesses.

<sup>1</sup> <https://www-nds.iaea.org/relnsd/vcharthtml/VChartHTML.html>

<sup>2</sup> Ichimiya, Narita, and Kitao, 1998

## 3 Experimental techniques and systems for aqueous chemistry

### 3.1 Kinematic pre-separators

Transactinide elements are produced in extremely small amounts and their production is accompanied by various by-products, which are mostly also unstable. Of course, the decay radiation of these by-products may hinder the detection of transactinide isotopes of interest.

A physical pre-separator can be implemented to the system to ensure physical pre-separation of the transactinide elements before the chemical separation will occur. Pre-separators are coupled with a GJT (for details on GJT systems see section 3.2) system and usually use gasses like helium (He), neon (Ne), argon (Ar) or hydrogen (H) as a fill, hence the term gas-filled separators.

Nuclear-reaction products are separated based on their magnetic rigidity. The collisions with the gas atoms lead to leaving the reaction products in average charge state. This state is proportional to the cube root of their atomic number (Rowe *et al.*, 2000)

#### 3.1.1 Berkeley gas-filled separator (BGS)

The BGS in the Lawrence-Berkeley National Laboratory (USA) is a gas-filled separator which uses He gas as a fill. It consists of three magnets in the  $Q_v$ - $D_h$ - $D$  configuration, where D stands for dipole, Q stands for quadrupole, the index  $h$  stands for horizontal focusing, and  $v$  for vertical focusing.  $D_h$  bends the beam to the beam dump, helping separate the beam from the fusion-evaporation residues (EVRs). The second dipole magnet further supports the separation of the EVRs (Rowe *et al.*, 2000). The configuration of the BGS is in figure 3.

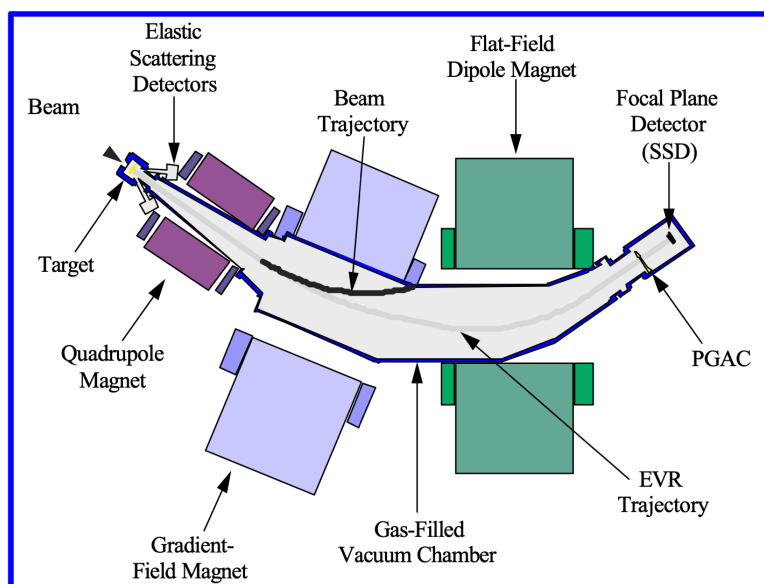


Figure 3: Schematics of the BGS. Adopted from (Rowe *et al.*, 2000)

#### 3.1.2 Transactinide separator and chemistry apparatus TASCA

The TASCA in the GSI Darmstadt (Germany) can operate in two different modes – High Transmission Mode (HTM) with the configuration  $D$ - $Q_h$ - $Q_v$  and a Small Image-size Mode (SIM) with the configuration  $D$ - $Q_v$ - $Q_h$  (Semchenkov *et al.* 2008). Figure 4 displays the configuration of the TASCA configuration.

Special recoil transfer chambers (RTCs) are designed for both modes. The RTC must have the smallest possible volume and dimensions, so that it can be flushed out as quickly as possible. However, it must also be wide enough to collect majority of EVRs and deep enough to thermalize all recoiling products.

The HTM provides the maximized transmission providing a more dispersed focal-plane image. This can be an advantage if focal plane detector is used. However, when a short-lived product is stopped in the RTC, because of large window area a large recoil volume is generated. Therefore, the flush time can be relatively long.

With SIM polarization  $Q_v$ - $Q_h$  is performed. This polarization provides smaller focal point than in the HTM mode. This results in allowing for a smaller RTC. Thus, faster flush time can be achieved. However, the transmission of this mode is cut down (Even *et al.*, 2002).

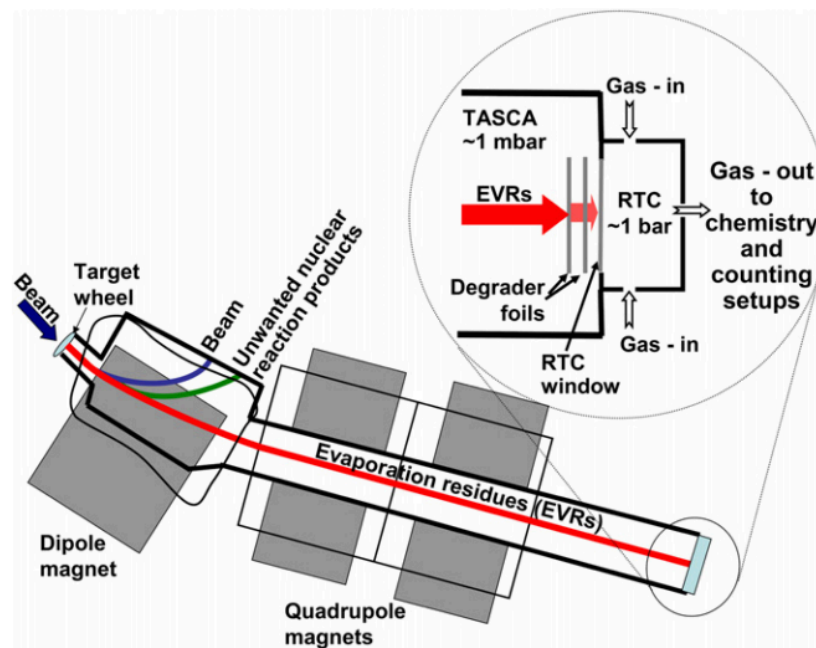


Figure 4: Schematics of the TASCA with detail of the RTC. Adopted from (Even *et al.*, 2011)

### 3.1.3 Dubna gas-filled recoil separator (DGFRS)

Gas filled separators are usually filled by He gas. However, the DGFRS in the Joint Institute of Nuclear Research (Russia) is filled by H gas as it provides better separation character than He in the case of fusion-evaporation reactions of heavy ions with actinide targets.

DGFRS is constituted of three magnets in configuration  $D_v$ - $Q_h$ - $Q_v$ . Horizontal and vertical quadrupole doublet is used for the focusing on the focal plane. The pressure of H gas inside the magnets is approximately 1 Torr (Subotic *et al.*, 2002). DGFRS configuration is displayed in figure 5.

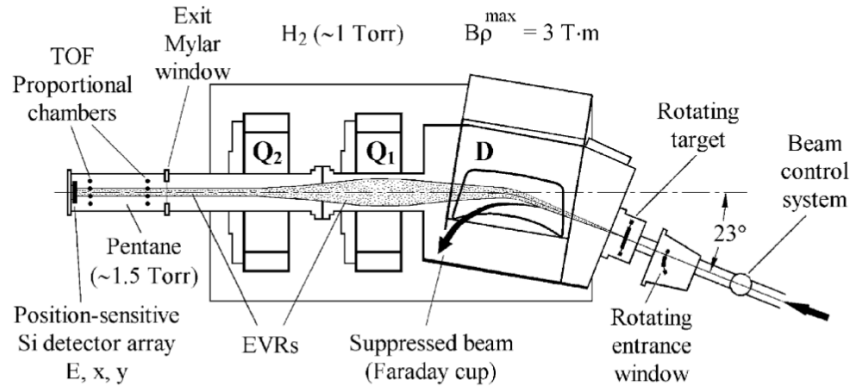


Figure 5: Schematics of the DGRFS (schematics is drawn opposite way than the rest of the gas-filled separators' schematics in this work). Adopted from (Subotic et al., 2002).

The DGRFS-II is an enhanced version of the DGRFS. The configuration of the DGRFS II is  $Q_v$ - $D_h$ - $Q_h$ - $Q_v$ - $D$ . Compared to the configuration of DGRFS,  $Q_v$  was added to the beginning, focusing of the  $D1$  was changed from vertical to horizontal and a  $D2$  was added to the end of the configuration. The  $D2$  was added to increase the separation efficiency (Oganessian, Utyonkov, Popeko et al., 2022).

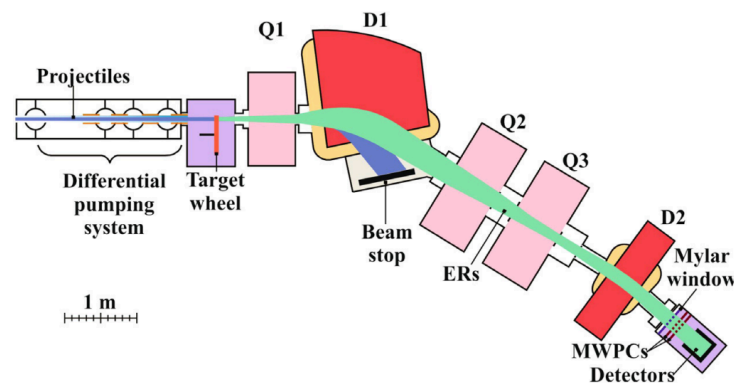


Figure 6: Schematics of the DGRFS-II. Adopted from (Oganessian, Utyonkov, Popeko et al., 2022).

### 3.1.4 Gas-filled recoil ion separator (GARIS)

The GARIS is implemented to the RIKEN linear accelerator (RILAC) facility in Japan. It consists of four magnets of configuration  $D_{vh}$ - $Q_h$ - $Q_v$ - $D$ , as (Morita, 2015) shown in figure 7.

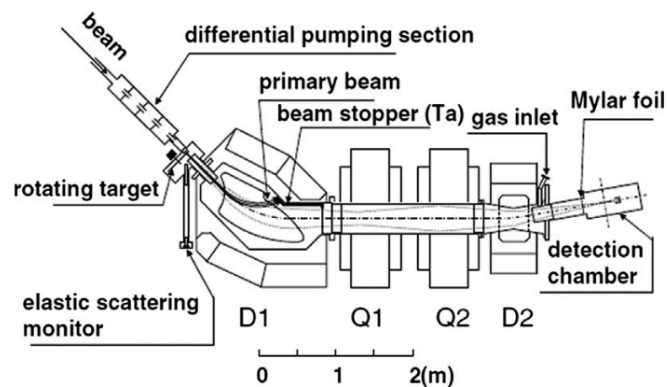


Figure 7: Schematics of the GARIS. Adopted from (Morita, 2015).



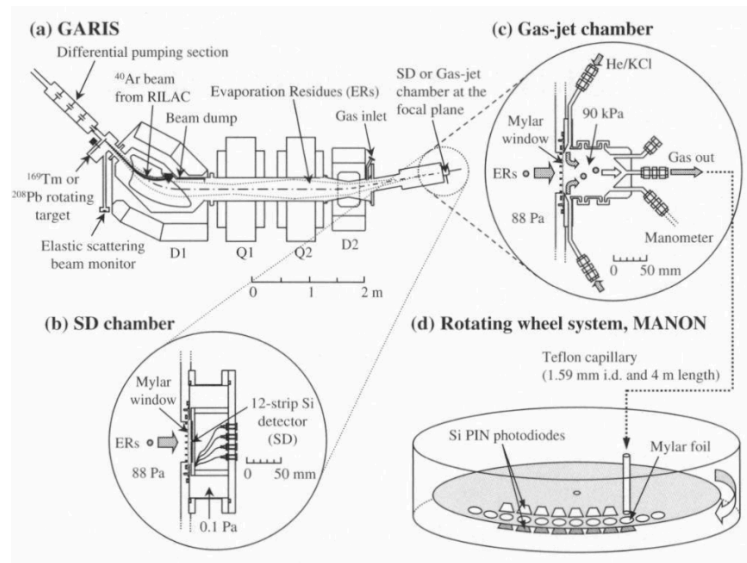


Figure 8: Schematics of the GARIS with the detail of the gas-jet chamber, a Si detector, and the MANON system. Adopted from (Haba *et al.*, 2007).

The D1 leads the beam to the beam dump and separates EVRs. However, some of the EVRs can come through the D1 and Qs and reach the focal plane. These EVRs would increase the background levels. Therefore, D2 is implemented to the system to reduce these background events and increase the resolution at the focal plane (Kaji, Morita, Morimoto *et al.*, 2003).

The GARIS-II, enhanced version of the GARIS, was implemented to the RILAC facility in 2013, consisting of five magnets. The configuration is  $Q_v$ - $D_h$ - $Q_h$ - $Q_v$ - $D$  (Kaji *et al.*, 2013), as displayed in figure 9. Configuration of the GARIS-II is the same as of the DGFRS-II. However, parameters differ as showed in table 3.

The first  $Q_v$ , providing vertical focusing, was implemented to the system to better match the acceptance of the D1. The rest of magnets has the same function as in the GARIS. Extra movable slit is applied to help reduce the background particles.

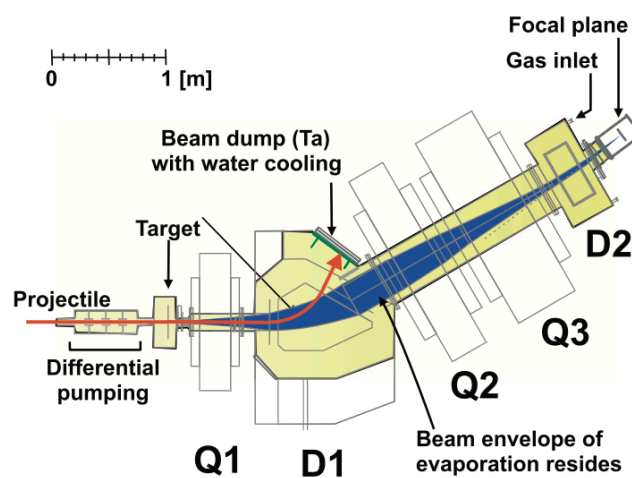


Figure 9: Schematics of the GARIS-II. Adopted from (Kaji *et al.*, 2013).

Table 3: Comparison of the data on known gas-filled separators. Adopted from (Oganessian, Utyonkov, Popeko et al., 2022).

Set-up	Scheme	Bend. angle	$B \cdot \rho_{max}$ T m	Dispersion mm/% $B \cdot \rho$	Length m
DGFRS-1	$D_v Q_h Q_v$	23°	3.1	7.5	4.07
BGS	$Q_v D_h D$	(25 + 45)°	2.5	20.0	4.6
GARIS-1	$D_{vh} Q_h Q_v D$	(45 + 10)°	2.16	9.7	5.76
TASCA	$D Q_h Q_v$	30°	2.4	9.0	3.5
GARIS-2	$Q_v D_h Q_h Q_v D$	(30 + 7)°	2.43	19.3	5.06
DGFRS-2	$Q_v D_h Q_h Q_v D$	(32 + 10)°	3.35	32.8	7.41

## 3.2 Gas-jet transport (GJT) system

A GJT system is used for fast transport and physical separation of isotopes (Silva *et al.*, 1977). The transport can be as fast as one second. A GJT system is constituted from a carrier gas, which ensures that the EVRs are stopped, stabilized, and then carried away by the gas flow from an RTC to an experimental set-up. There are several types of GJT systems depending on the type of carrier gas used and whether the gas is used pure or seeded with aerosol particulates.

For non-volatile products, inert gas seeded with solid aerosol particulates (mainly halide salt or carbon) is used (Bartl, Běhal, Matlocha, *et al.*, 2023). More detailed information on aerosol GJT systems is in section 3.2.1. For volatile products, pure inert gas, or mixture of inert gases are usually used. However, the inert gas or the mixture can be also infused with reactive gas to form volatile species (Bartl, Běhal, Matlocha, *et al.*, 2023).

A GJT system is composed of a high-pressure gas source, which can be a gas generator or a gas cylinder. A mixing valve can be implemented in order create the gas mixtures. Gas delivery system, which contains components such as flowmeters, oversee regulation of the flow rate of the gas and the pressure. For aerosol seeded GJT system, an aerosol generator is connected to the system. Aerosol generators are further described in the section 3.2.1. Another part of a GJT is a nozzle. When the flowing gas passes through the nozzle a gas jet is formed. Depending on the nozzle properties, such as shape or size, the gas jet properties are determined. In an RTC the gas jet and the EVRs are introduced. EVRs are then transported to the experimental set-up.

### 3.2.1 Aerosol GJT system

System consists of two parts – carrier gas and aerosol particulates for seeding the gas.

The carrier gas is an inert gas, usually He or Ar, at a pressure above one bar. (Wollnik, 1976) It serves for stabilization and fast transport of the recoiled products. Helium is mostly favoured for longer recoil ranges.

In the aerosol GJT system, an aerosol generator is implemented. Depending on the type of aerosol, different approaches are used for its generation.

For generating the salt aerosol particulates, e.g., KCl, a tube furnace filled with KCl is used. Due to the heat induced by the furnace, KCl gets sublimed. As the KCl vapours mix with the carrier gas, they cool down and the salt vapour desublime forming particulates of around 100 nm in diameter (Wollnik, 1976).

Carbon aerosols are generated by a spark discharge between two graphite electrodes. The discharge causes the carbon particles to vaporize and aggregate upon cooling in the carrier gas, forming particulates of around 92 nm in diameter (Eibach *et al.*, 2010).

In the RTC, products are introduced to the carrier gas seeded with aerosol particulates. The product particles (EVRs) get stabilized in the gas, adsorb onto the aerosol particulates, and are transported through a capillary to the experimental set-up.

The efficiency of such GJT system can be over 50 % for distances over 20 m. The high efficiencies can be explained through Bernoulli's law and the laminar flow (Türler, Gregorich, 2013) – according to the profile of laminar flow, the pressure is higher the closer the distance to capillary wall. The velocity of the flow is decreasing the closer the particle is to the capillary wall. Therefore, the highest velocity is in the centre of the capillary. If the particle of aerosol with the products deviates from the centre of the capillary, restoring force pushes it back towards the centre.

### 3.2.2 TRIGA-SPEC facility

Experimental setup at TRIGA-SPEC uses the carbon-aerosol seeded gas in their GJT system to carry EVRs from the TRIGA reactor. A scheme of the GJT set-up is displayed in figure 10. Helium serves as the carrier gas and makes up the inert atmosphere surrounding pure graphite electrodes. A capacitor is connected to pure graphite electrodes and is being constantly charged. When the capacitor reaches the breakdown voltage of 1.5 kV, a spark discharge occurs between the electrodes leading to the release of some carbon material. Immediately after the release, carbon fumes cool down and desublime, forming solid particulates of mean diameter of 92 nm (the size distribution curve is shown in figure 12) (Eibach *et al.*, 2010). Particulates are released into the He-gas flow leading through a tube filter to the RTC. The set-up is equipped with a tube filter to prevent light and heavy aerosol particulates from blocking the transport capillary. Sedimentation and diffusion processes take place in the tube filter. After being released from the target, the EVRs are stopped in the He gas, adsorbed onto the carbon particles, and then transported through a capillary to the experimental set-up, where He is removed, and aerosol particles are separated from the fission (recoil) products. The advantage of carbon aerosol is easy production and favourable properties for mass spectrometry as the atomic unit is 1/12 of the mass of  $^{12}\text{C}$ .

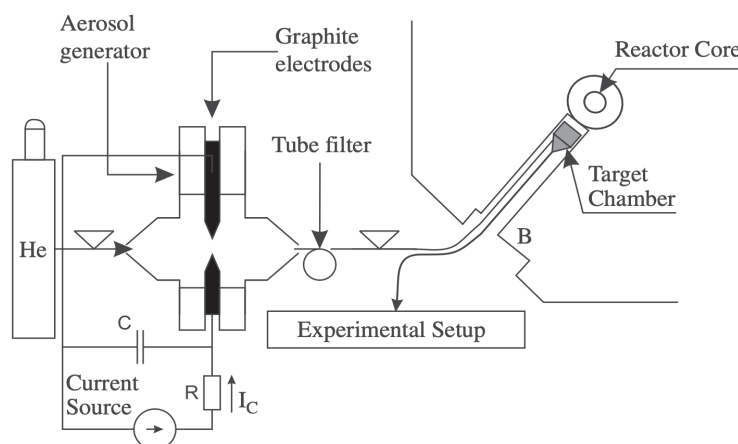


Figure 10: Schematics of the TRIGA-SPEC gas-jet system with pure graphite electrodes for production of carbon aerosols. Adopted from (Eibach *et al.*, 2010).

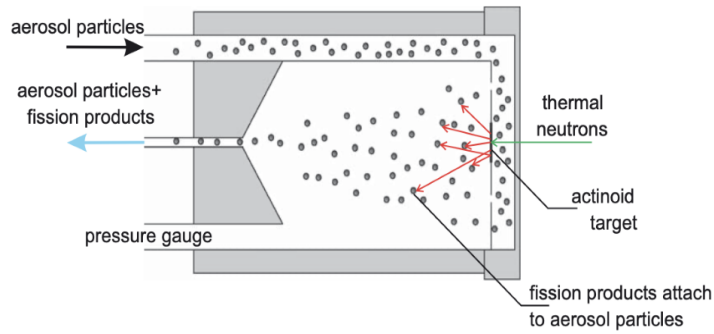


Figure 11: Schematics of the TRIGA-SPEC target chamber, where carbon aerosol gas-jet is introduced to the chamber as close to the target as possible. Adopted from (Eibach et al., 2010).

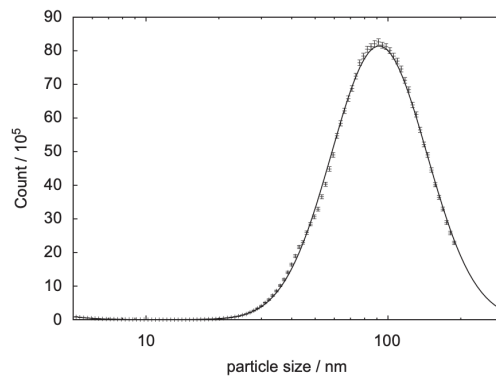


Figure 12: Distribution of the size of carbon aerosol particles produced by the graphite electrodes at the TRIGA-SPEC. Mean diameter is approximately 92 nm. Adopted from (Eibach et al., 2010).

### 3.2.3 SINQ (Swiss spallation neutron source) facility

The SINQ facility provides versatile solution for supplying various species of interest via a GJT system. As displayed in figure 13, up to four gasses can be used for the carrier gas (or in a mixture) in the SINQ facility. Different GJT system types are provided through paths 1-3, as shown in the figure 13. Path 1 is equipped with a tube furnace with halide salt for generating the salt aerosol particulates. Path 2 is a clear capillary used for pure-gas-based GJT. Path 3 contains carbon electrodes with spark-discharge source to generate carbon aerosol particulates. As mentioned in section 3.2.1, paths 1 and 3 are used for aerosol seeding of the carrier gas to transport non-volatile EVRs (Tiebel, Dutheil, Dressler et al., 2022).

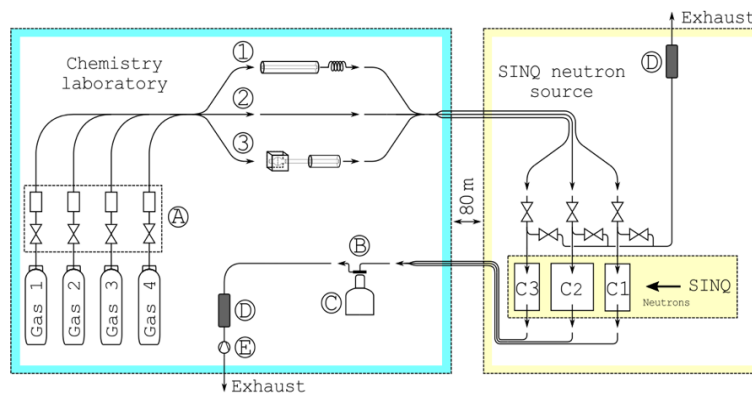


Figure 13: Schematics of the GJT between the laboratory and the SINQ source at the PSI. For details see the text. Adopted from (Tiebel, Dutheil, Dressler et al.).

### 3.3 Dissolution techniques

#### 3.3.1 Preconcentration and washing out

To achieve more accurate measurements of the desired radionuclides, short preconcentration step may be employed. This technique is used in systems utilizing chromatographic columns, such as automated rapid chemistry apparatus (ARCA), ARCA-II and automated ion-exchange separation apparatus coupled with the detection system for alpha spectrometry (AIDA). ARCA provided solid base for the development of ARCA-II and later of AIDA.

In ARCA system, aerosols are transported by the GJT system and collected on a frit. Depending on the position of the sliders, different steps of the separation are executed. In one position of the sliders, KCl particulates are collected on the frit and residual gases are pumped away. In the next sliders' position, liquid solvent is flowing through the frit, dissolving the products, and carrying them to the chromatographic column, where the separation step takes place. Further path of the eluent is again decided by the sliders. Eluent can be driven either to the waste, test tubes placed in a fraction collector, to the next column to execute further separation, or (the eluent containing EVRs) caught on a hot tantalum (Ta) disk, where the aqueous solution is evaporated for upcoming  $\alpha$  spectrometry measurements. Vacuum chambers equipped with large area passivated implanted planar silicon (PIPS) detector, to which the sample needs to be transported manually, are used for  $\alpha$  spectrometry in the case of the ARCA (Schädel *et al.*, 1988). Hence, detection is performed in a semicontinuous mode. Schematics of ARCA system is displayed in figure 14.

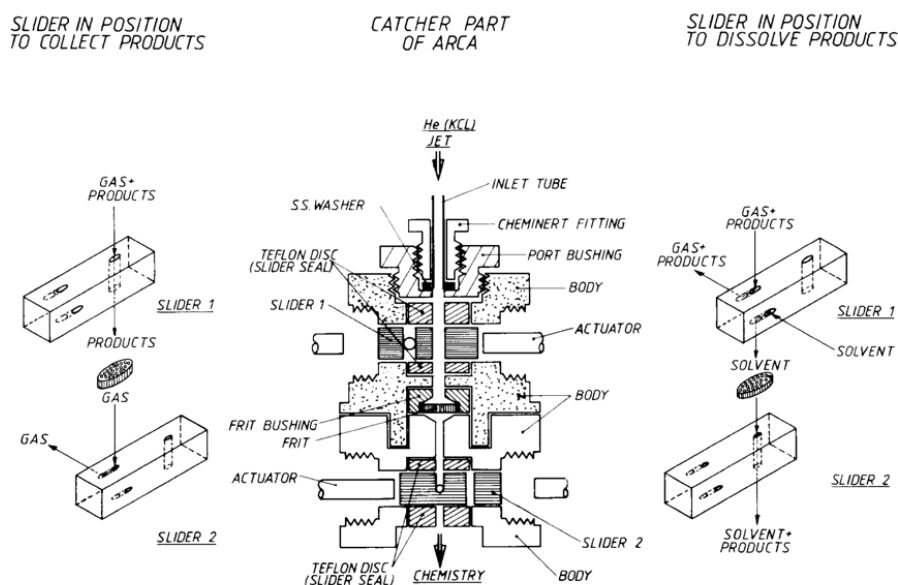


Figure 14: Schematics of the catcher part of the ARCA with details on sliders. Adopted from (Schädel, Brüchle, Jäger, Schimpf, Kratz, Scherer and Zimmermann, 1989).

The ARCA-II is an improved version of the ARCA. The liquid chromatography system consists of two magazines of twenty ion-exchange microcolumns (8 mm long). The magazine with columns moves by one position each time it is used. This process prevents the cross-contamination between the samples. The presence of two magazines ensures the maximum readiness for the separation, as they can operate simultaneously (Schädel *et al.*, 1989). This feature gave the base for the development of AIDA.

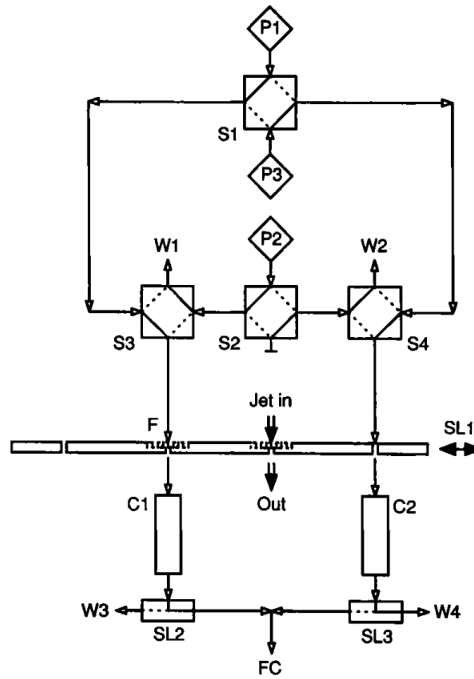


Figure 15: Schematics of the ARCA-II components. Adopted from (Schädel, Brühle, Jäger, Schimpf, Kratz, Scherer and Zimmermann, 1989).

In AIDA, two different paths, as shown in figure 17, for the supply of solutions are available. In the first path, the eluent goes through the collection site to the microcolumn. In the second one, the solution is directed to the column after one-step forward movement of the column magazine to avoid cross-contamination at the collection site. Sample preparation for  $\alpha$  spectrometry is similar to the ARCA II, but in the case of AIDA, samples collected on Ta plates are automatically moved to vacuum chambers housing PIPS detectors (Nagame *et al.*, 2005).

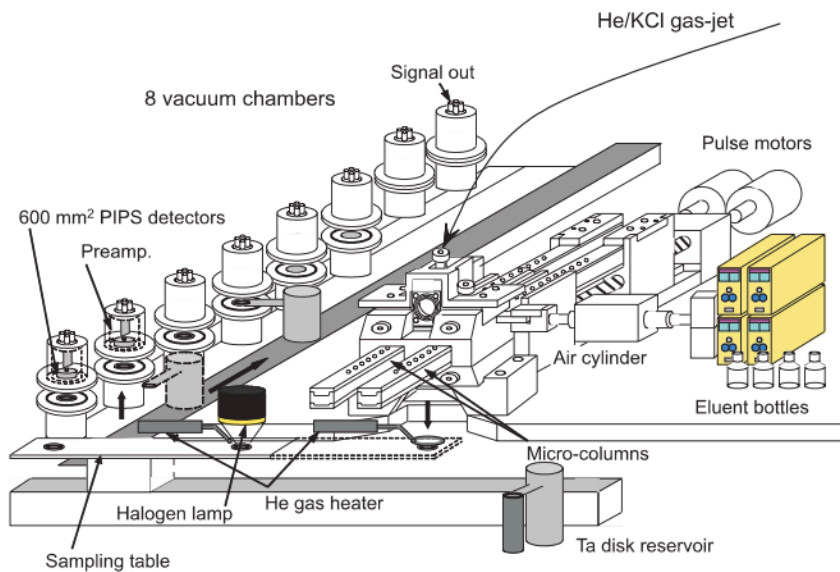


Figure 16: Schematics of the AIDA. Adopted from (Nagame *et al.*, 2005).

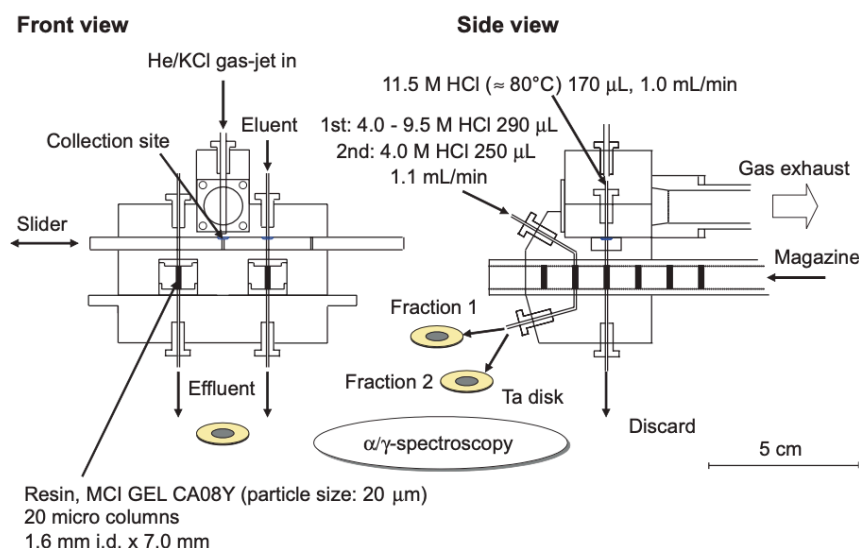


Figure 17: Schematics of the modified ARCA system within the AIDA. Adopted from (Nagame *et al.*, 2005).

### 3.3.2 Stationary mixer and degasser centrifuge

The system of a stationary mixer and a degasser centrifuge is used in, e.g., SISAK system (Aronsson *et al.*, 1974), which is an on-line extraction apparatus constructed as a system of mixers and centrifuges (see Fig. 16). The EVRs are delivered to the system via an aerosol seeded GJT system. The gas-jet is mixed with an aqueous solution in the stationary mixer, which is implemented to the system in order to boost dissolution rate. The stationary mixer is placed ahead of each centrifuge inlet. The centrifuges have very small volumes (around 0.3 mL) and high flow rates (up to  $2 \text{ mL s}^{-1}$ ) to ensure short transport times (Omtvedt *et al.*, 1998). Aqueous solution containing the dissolved aerosols with EVRs is intermixed with organic solution in the stationary mixer. The phases are separated in a separation centrifuge. Scintillation cocktail is then added to the pure organic phase (while the pure aqueous phase goes to the waste), and the solution is pumped in the detection cells, where liquid scintillation  $\alpha$  spectrometry is performed on the sample.

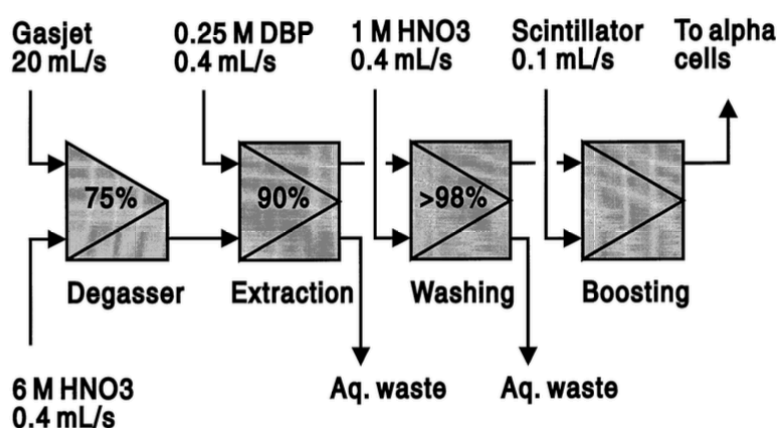


Figure 18: Schematics of the SISAK set-up with yield indicated for each step. Adopted from (Omtvedt *et al.*, 1998).

### 3.3.3 Membrane degasser (MDG)

The MDG is equipped with semipermeable hydrophobic Teflon membrane, which allows for the gas to pass through, while the aqueous solution stays in the MDG channel. Aerosols from the GJT system

and the aqueous solvent are introduced in the stationary mixer. For higher mixing efficiency, two crossings of the gas and aqueous phases are carried out in the mixer (Ooe *et al.*, 2015).

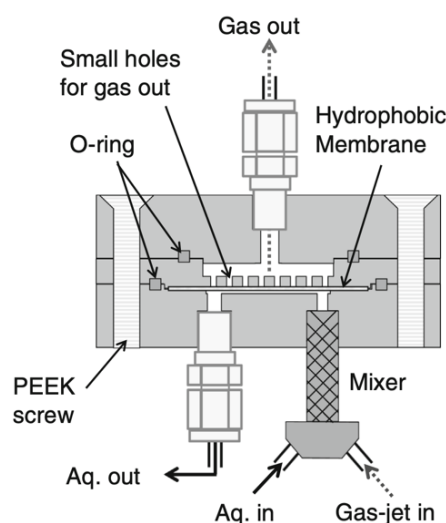


Figure 19: Sectional view of the MDG with description. Adopted from (Ooe *et al.*, 2015).

### 3.3.4 Particles-into-liquid sampler (PILS)

The PILS serves as a transition step from high-flow-rate GJT system to a low-flow-rate aqueous stream (Weber *et al.*, 2001, Orsini 2003). The GJT system is brought into a conical chamber filled with supersaturated water vapour, which is generated by a steam generator. Solid aerosols gradually turn into droplets as they pass through a system of cooling ribs, while condensation occurs onto their surface. The droplets pass through the jet nozzle into the impactor chamber, where the gas is pumped out. Droplets are collected on the quartz impactor plate, which is continuously washed by the aqueous phase. Washed liquid continues to the debubbler unit, where it is separated from residual gas. The aqueous phase, now containing the dissolved EVRs, is then ready for further processing (Bartl, Němec, Zach *et al.*, 2023).

## 4 Continuous detection techniques

In case of short-lived nuclei, standard approach to detection might not work as it can be time consuming and the species of interest might decay before the detection step is finished. Also, the detection technique may not be sensitive enough. For this reason, it is needed to work fast and efficiently, or to use continuous detection techniques.

### 4.1 Detection of transactinides

For detection of transactinides,  $\alpha$  spectrometry or liquid scintillation spectrometry have been used. To improve the detection sensitivity, both techniques are often used in coincidence with X-ray or gamma-ray detection techniques.

#### 4.1.1 Alpha spectrometry

In general, alpha spectrometry is usually a non-continuous detection technique. It is valued for its high energetic resolution. Alpha spectrometry can be used for both, qualitative and quantitative analyses. However, the technique is experimentally demanding even in semi-continual implementation, as  $\alpha$ -particles are particles of short-range, which complicates their detection.



AIDA, mentioned in section 3.3.1, is coupled with PIPS  $\alpha$ -particle detectors that are supplied with the samples by a conveyor belt to ensure fast delivery to the detection step. However, the samples for the  $\alpha$  spectrometry are prepared on solid Ta disks that provide only  $2\pi$  detection geometry. More details about AIDA and its configuration can be found in Nagame *et al.*, 2005.

The MANON (measurement system for alpha particle and spontaneous fission events on-line) can be used instead of Ta disks for detection of  $\alpha$ -particles and fission products. The  $\alpha$ -particle detection in MANON is more efficient. The MANON is equipped with a thin catcher foil, instead of the Ta disks. Aerosols with desired EVRs, transported by GJT system, are lead through a Teflon capillary onto a catcher foil (polyethylene terephthalate of thickness of approx.  $120 \text{ g cm}^{-2}$  and diameter of 20 mm), which is attached to a wheel. The wheel is rotated after specific period and moves the catcher foil between six pairs of Si PIN photodiodes, that are located above and below the catcher foil, i.e., making a nearly  $4\pi$  detection geometry (Nagame et al, 2003). However, this system have not been optimized for the use with liquids.

### 4.1.2 Liquid scintillation

The liquid scintillation spectrometry has high efficiency, but its energy resolution is relatively low. For this reason, emphasis is placed on precise sample pre-treatment and detection settings, depending on experiment carried out.

Organic liquid scintillator using dimethyl-POPOP and naphthalene dissolved in toluene is utilized in the SISAK system for measurements of the organic phase (containing an extracting agent, di-(2-ethylhexyl)-phosphoric acid or dibutyl phosphate). At the output, organic phase, containing the species of interest, is lead to a spherical quartz detector cell, which is coupled with a photomultiplier. Three such detector cells in series (connected by delay loops) were implemented in the SISAK system. More details about the LSC system used in SISAK is available in Wierczinski *et al.* (1995).

Liquid scintillation can achieve basically full  $4\pi$  measuring geometry, which is a great advantage for any measurements, but especially for measurements with low count rates and of charged particles. The interference with  $\beta^-$  (and  $\gamma$ ) is corrected for through electronic pulse discrimination and pile-up rejection.

## 4.2 Continuous gamma detection – residence time distribution

### 4.2.1 Residence Time Distribution (RTD)

No chemical system can be considered ideal. One of the possible ways to describe the non-ideality of a radioactive material behaviour in a flow-through system is the residence time distribution (RTD). This concept is used for the description of the flow-through dynamics and various deviations in flow and mixing. Using ideal models, the RTD is used as a higher approximation to achieve better results for the non-ideal flow, which occurs in the real chemical reactors. In case of the usage of radiotracers, usually a continuous gamma detector is used to determine the RTD, as it can provide real-time information about the system.

#### 4.2.1.1 Measurement of the Residence Time Distribution

Experimental measurement of the RTD is done by injecting tracer into the system. Tracer is a chemical, molecule or atom which helps to track and understand the behaviour of a substance in the reactor. The tracer is injected at the time  $t = 0$ . The concentration of the tracer is measured at the outlet at

different times. Important properties of the tracer are to be inert, easily detectable, soluble in the mixture inside the reactor and with similar physical properties to the mixture. Furthermore, the tracer should not be adsorbed on the surface of the reactor. Usually dyes and radioactive chemicals are used as tracers. For the methods of injecting the tracer, pulse input and step input are used the most (see figure 20).

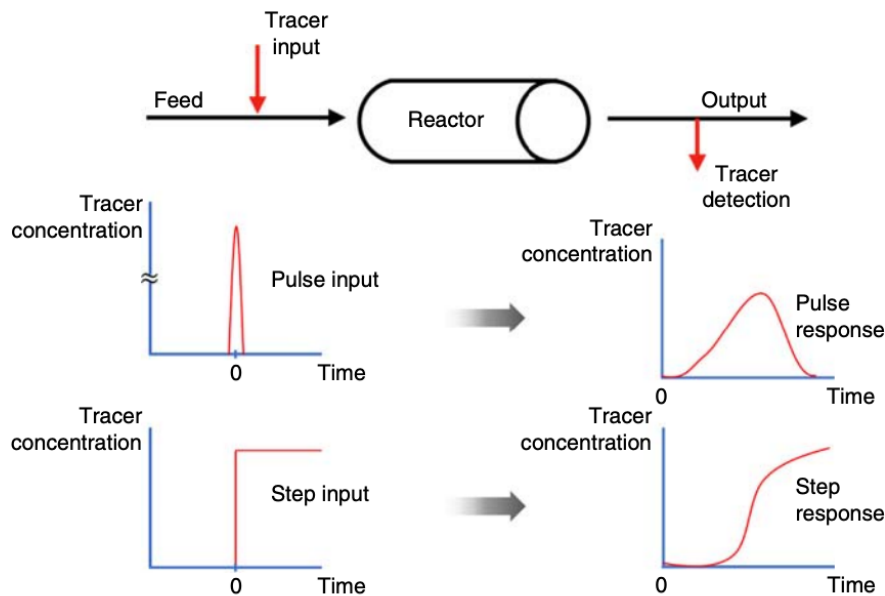


Figure 20: Illustration of differences between the pulse input and the step input methods. Adopted from (Conesa, 2019).

#### 4.2.1.2 Pulse Input

The tracer is injected into the stream flowing into the reactor in as short time as possible, forming a very sharp input that can be ideally described by the Dirac delta function and approximated by a peak function. The concentration of the tracer at the outlet is measured as a function of time, as the sharp Dirac-delta-like input gets naturally spread into a residence time distribution.

The pulse input may be challenging as the injection pulse time should be considerably shorter than the residence time of the tracer inside the reactor. Also, the tracer dispersion between the injection site and the reactor's inlet must be negligible. However, if these conditions are met, the pulse input technique is a great and relatively direct way to obtain RTD (Conesa, 2015).

#### 4.2.1.3 Step Input

In the case of the step input, the injection of a tracer is also sudden, but its concentration supplied to the system remains constant during the whole experiment to create a step. Such input can be ideally described by the Heaviside step function and can be approximated by a sigmoid function. Compared to pulse input method it is easier to experimentally execute the step input method as it does not require the knowledge of exact amount injected. However, this method comes with drawbacks; The maintenance of the constant concentration supply can be complicated and since the supply is constant, great amounts of the tracer are used, which can be mainly a financial challenge (Conesa, 2015).

## 4.2.2 Continuous gamma detection

Gamma-rays can be detected by gamma spectrometry. This technique can be operated continuously, which is valued in studies of short-lived radionuclides. Gamma spectrometry is a technique used to identify and quantify radionuclides by detecting the emitted  $\gamma$ -rays of specific energies.  $\gamma$ -rays are usually highly penetrating and can be easily detected using high-resolution detectors, e.g., HPGe detector. Another possibility for measuring the  $\gamma$ -rays is an inorganic scintillation detector, such as NaI:Tl, which does not generally reach as high resolution as HPGe detector, but the operation and handling of the detector are very simple. Gamma spectrometry usually requires minimal sample preparation, contrary to alpha spectrometry. (Wolf, 2008).

### 4.2.2.1 HPGe

HPGe semiconductor detectors offer high energy resolution of  $\gamma$ -spectrums compared to inorganic scintillation detectors. However, a big disadvantage of these detectors is that they require cooling to reduce electronic noise and improve their energy resolution. The most common cooling method involves using liquid nitrogen to maintain the detector at cryogenic temperatures (Němec, Čubová, Semelová, Bartl, 2020).

HPGe detectors are overall more complex and expensive compared to inorganic scintillation detectors (like NaI:Tl), primarily due to the cooling requirements and the high-purity germanium material needed for their construction.

### 4.2.2.2 NaI:Tl

NaI:Tl detectors offer high sensitivity to  $\gamma$ -rays. They are widely used for their affordability, availability of different sizes, and favourable detection conditions (operates at room temperature). NaI:Tl detectors may provide very fast, real-time detection response, enabling thus continuous gamma detection.

However, NaI:Tl detectors do have their limitations. Their energy resolution is considerably lower when compared to HPGe detectors. This limitation can make it more challenging or simply impossible to distinguish between gamma rays of close energy levels. Additionally, hygroscopic nature of NaI:Tl crystals can also pose concerns, as they have the tendency to absorb moisture from the environment, influencing their long-term performance (Němec, Čubová, Semelová, Bartl, 2020).

## 5 Experimental

### 5.1 Cyclotron U-120M

The U-120M cyclotron (NPI CAS, Czech Republic) is capable of accelerating various positively charged particles in the energy levels ranging from 1 to 55 MeV. In this work,  $^3\text{He}$  beam is used for reactions with the gold-metal foil target, leading to the generation of desired radionuclides. The cyclotron's beam current varied between 100 and 500 nA, while the energy of the beam was between 40 and 52 MeV.

For this work, radionuclide  $^{195\text{m}}\text{Tl}$  was utilized. This radionuclide is obtained through collision of the  $^3\text{He}$  beam with the  $^{197}\text{Au}$  target foil according to the reaction (1).



From RTC the formed EVRs are carried by the GJT for further processing.

### 5.2 Modular robotic gas-jet target system (MARGE)

MARGE system ensures the remote exchange of the target foils. In addition to reducing the time required for manual target foil exchange, the MARGE system is also equipped with an automatic screen shutter/lifter. The screen is used for the rapid stopping of the beam of accelerated particles, thus stopping the influx of new EVRs or lifting the screen and letting the beam interact with the target foil (Bartl, Běhal, Matlocha *et al.*, 2023). More detailed description of the MARGE system is in Bartl, Běhal, Matlocha *et al.* (2023).

### 5.3 Recoil transfer chamber and gas-jet transport system

The transport of radionuclides generated at the cyclotron to the laboratory is performed by a GJT system, which was developed at Oslo Cyclotron Laboratory (UiO, Norway) and implemented into the new MARGE target, recoil, and transport system (Bartl, Běhal, Matlocha *et al.*, 2023). This schematic of the Oslo GJT system is on figure 21; the system employs a highly efficient He-jet stream that carries dispersed KCl aerosols to adsorb and transport the cyclotron-produced radionuclides.

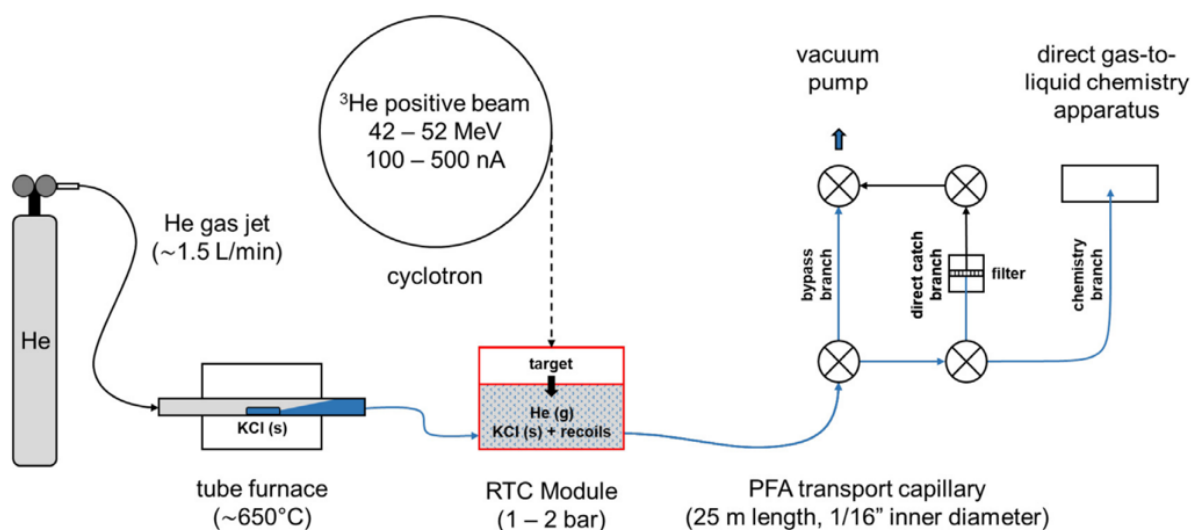


Figure 21: Schematics of the Oslo GJT system. Adopted from (Bartl, Běhal, Matlocha *et al.*, 2023).

The KCl aerosols are produced by subjecting KCl powder to controlled heating in a tube furnace (Nabertherm, Germany). The tube furnace diligently operates at temperatures around 650 °C, ensuring the optimal conditions for formation of the desired aerosols.

Once formed, aerosols are transported by the He-jet stream, with usual operating flow rate ranging from 1.0 L min<sup>-1</sup> to 1.5 L min<sup>-1</sup>, to the recoil-transfer chamber (RTC). In the RTC, the process of recoil from the target takes place. Recoiled products are subsequently stabilized in the He gas and adsorbed onto the KCl particulates. He-jet carries the adsorbed recoil products through a system of pneumatically controlled valves to a designated destination within the laboratory.

Valve system ensures dynamic routing of the He-jet based on the requirements of specific experiments. In the case of absence of ongoing experiments, He stream is directed through the bypass branch, which leads directly into the vacuum pump outlet.

In the majority of experiments, the He-jet is lead into the direct catch branch, where the aerosols are collected on a glass microfiber filter (Whatman GF/C) and the filtered He stream continues to the vacuum pump outlet.

Alternatively, He stream can be directed into the chemistry branch. In this configuration, the helium stream is channelled directly into an open capillary, which can be attached to a gas into liquid chemistry apparatus.

## 5.4 Gas mixing chambers

The PILS device (for details see section 5.5) was designed for much higher gas flow rates (16 L min<sup>-1</sup>) than are achieved in this experiment. As a compensation, inflowing gas-jet is mixed with air to achieve the desired flow rate. To achieve homogenous gas mixture, a mixing chamber was implemented to the system.

### 5.4.1 Glass mixing chamber

This mixing chamber was originally developed for mixing liquids. However, even though it is far from ideal, it was used for mixing gasses. The air inlet had volume of approx. 7.5 mL, the GJT system inlet had volume of approx. 2 mL, and the PILS outlet had volume of approx. 8.5 mL. The volume of the mixing chamber was approx. 78 mL. The total volume of the glass mixing chamber was approx. 96 mL. The glass mixing chamber is displayed in figure 22.

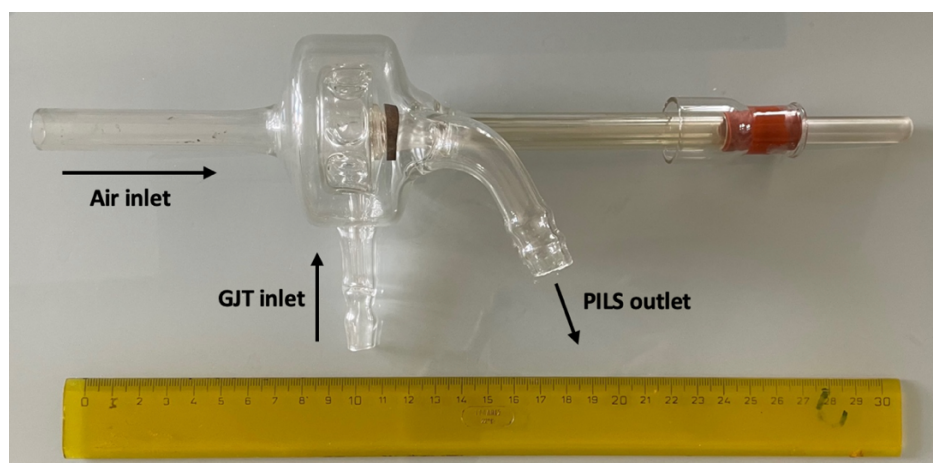


Figure 22: Glass mixing chamber with described inlets and outlet.

## 5.4.2 Gas mixer

The Gas mixer (Bronkhorst, Netherlands) is equipped with a small check valve which allow for precise and homogenous mixing of the two gases prior the PILS. The gas mixer is displayed in figure 23.

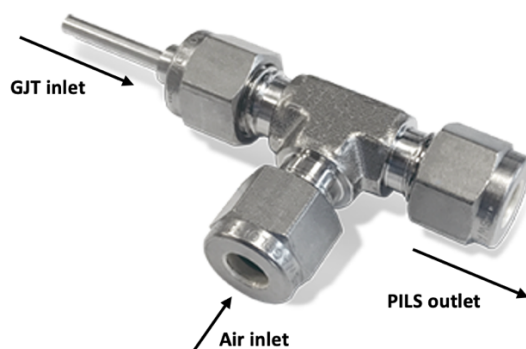


Figure 23: Gas mixer with described inlets and outlet.

## 5.5 Particles-into-liquid sampler (PILS)

The conversion of a high-flow-rate gas jet into a low-flow-rate aqueous stream is ensured by integrating the commercially available ADI 2081 Particle-Into-Liquid Sampler (PILS) (MetrOhm, Switzerland) into the system. This cutting-edge PILS device was originally developed for concentrating airborne aerosols as a sample pre-treatment for ion chromatography.

KCl-containing He-jet is introduced to supersaturated water vapor. Within this highly saturated environment, while passing over the cooling ribs, water vapor condenses on the surfaces of the KCl particulates, transforming them into droplets. These micro droplets are channelled through a jet nozzle, directing them into an impactor chamber. As they pass through the chamber, droplets are caught on an impactor plate, which is continuously washed by an aqueous phase. The carrier gas undergoes an expansion and is pumped away.

The aqueous solution, carrying the dissolved aerosols, is then directed into a debubbler unit, where any lingering traces of gas phase are separated from the solution. The gas-free aqueous solution is ready to undergo further processing. A schematic of the PILS system is showed in figure 24.

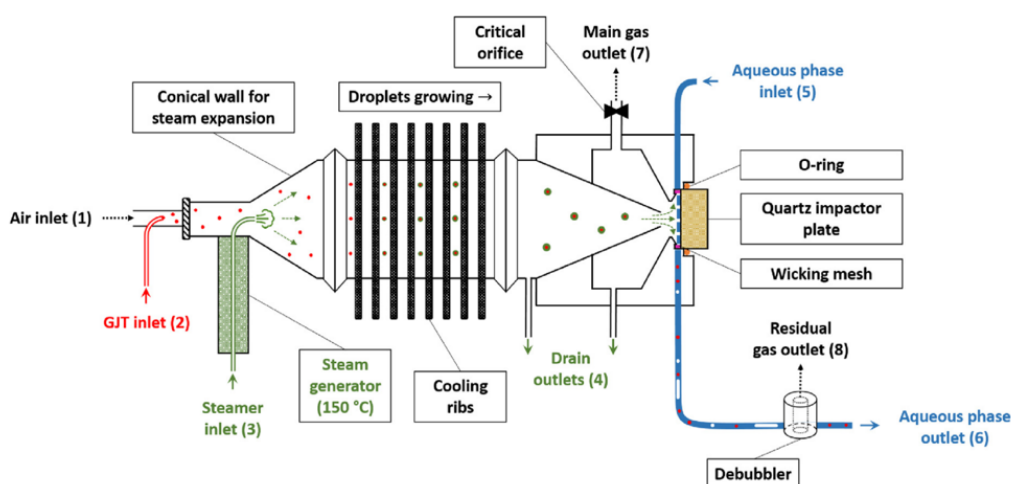


Figure 24: Schematics of the PILS with the GJT system inlet and a debubbler. Adopted from (Bartl, Němec, Zach et al., 2023).

## 5.6 Detection

The measurement of the transport time from the RTC to the impactor quartz plate (head) of the PILS was performed by a 2 x 2" NaI:TI scintillation probe (Nuvia, Czech Republic) with a DigiBase analyser (Ortec, USA). Configuration can be seen in figure 25. Foam pad was used to protect both devices and to moderately reduce the noise.

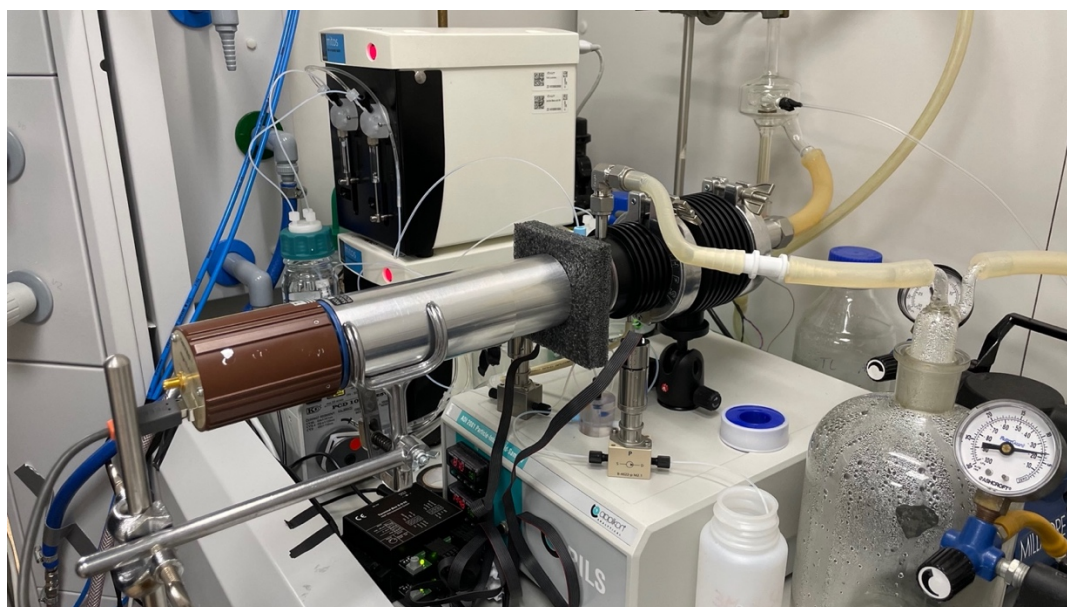


Figure 25: Photo of the experimental setup for measuring of the transport time from the RTC to the PILS.

Different types of measuring geometries were tested. However it was opted out for measuring at the PILS head (the back of the impactor plate), mainly because of the short-lived nature of measured  $^{195\text{m}}\text{Tl}$  and possible appearance of dead volumes.

During the measurement no shielding was used. Several consecutive spectra were collected with the measuring time of 1 s. The dynamics of the  $^{195\text{m}}\text{Tl}$  in the PILS impactor chamber, i.e., its accumulation towards a stationary state and its flushing out was measured by turning the  $^3\text{He}$  beam on and off. This was achieved by putting a solid beam monitor in and out of the beamline (details on the beam monitors can be found in Bartl, Běhal, Matlocha *et al.* (2023)).

Furthermore, the dynamics of the  $^{195\text{m}}\text{Tl}$  in the aqueous phase should have been tested. However, simple measurements on the aqueous output capillary did not provide any signal due to the very short half-life and slow aqueous flow rate. Another tested geometry was a spiral shape to enhance the measurement volume. Capillary (outer diameter 4.0 mm, inner diameter 2.0 mm, length 520 mm, volume 6.534 mL) was embedded in a 3D printed (MK-3 Prusa, Czech Republic) guiding disk, which was designed in OpenSCAD specially for this experiment (see figures 26 and 27). However, when applied on the  $^{195\text{m}}\text{Tl}$ , the measurement was also physically inachievable. Dead volumes at the capillary inlet and the outlet as the capillary was bent to enter the 3D guide are also an issue for any further application. On the other hand, this spiral geometry may be useful for measurements of different radionuclide with slightly longer half-life as its accumulation in the detection volume could actually be significantly higher than its decay.

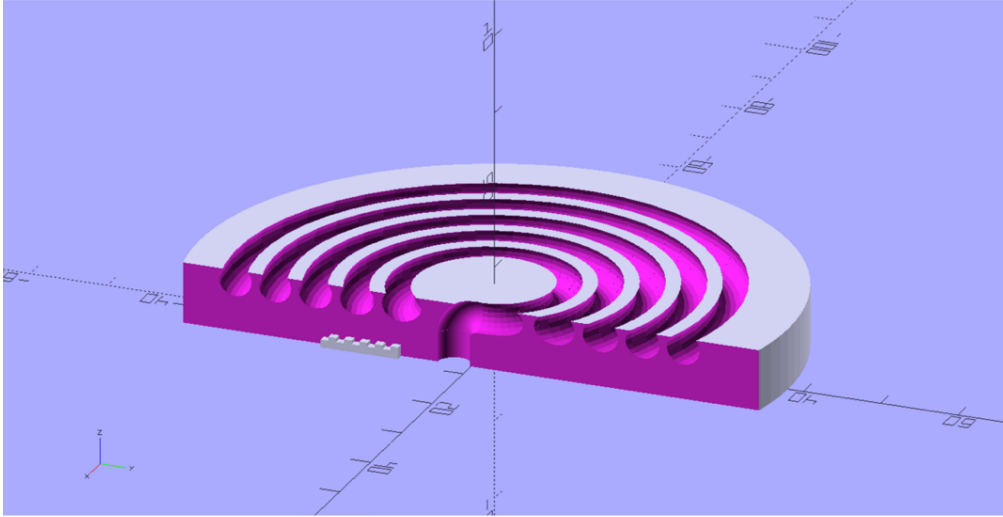


Figure 26: Sectional view of the 3D guiding disk for capillary.

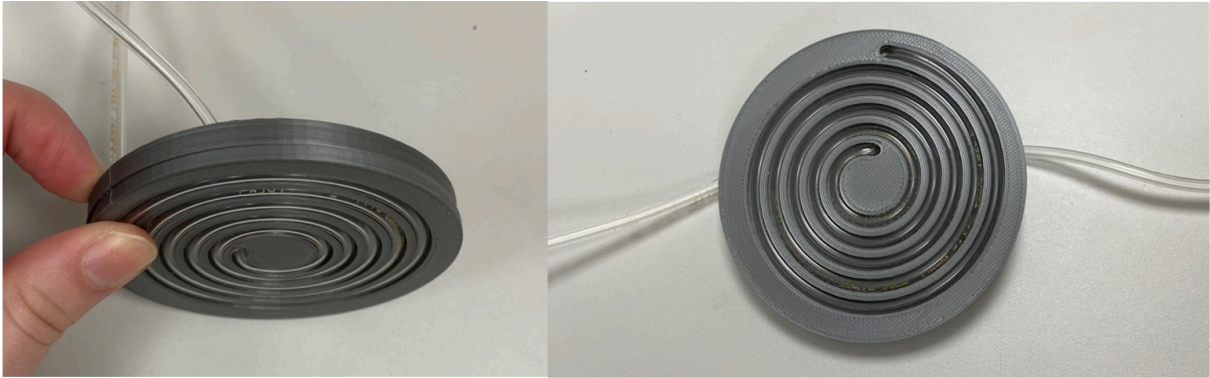


Figure 27: Printed 3D guiding disk with a capillary embedded to it.

## 5.7 Statistics

The MAESTRO software provided the information about the measured spectra, such as net area (NA), error of NA, gross area (GA), and number of channels  $n$  (width of the peak at its basin).

During the data treatment, the error propagation law (2) was applied to calculations of errors.

$$\sigma = \sqrt{\sum_i \left( \frac{\partial f}{\partial x_i} \cdot \sigma(x_i) \right)^2} \quad (2)$$

Critical value ( $L_c$ ) (3) was used to determine, whether the obtained data were clearly distinguishable signal ( $L_c < NA$ ), or the signal was distinguishable from noise ( $L_c \geq NA$ ).

$$L_c = \frac{1.645}{2} \cdot \sqrt{(GA - NA) \cdot 2 \cdot (n - 2)} \quad (3)$$

In equation (3), number 1.645 represents the quantile of standard normal distribution at 95 % confidence level,  $n$  is the number of channels which belong to the selected section and GA and NA represent the area of the peak of interest (DeFelice *et al.*, 2017).



## 6 Results and discussion

### 6.1 Data pretreatment

For  $NA$  values lower than corresponding  $L_C$  values, a mean of  $L_C$  values was calculated for each measurement set. This mean  $L_C$  was set as a noise baseline and was subtracted from all  $NA$  values within the set. By this operation, clear signal  $NA^*$  values and its error values  $\sigma_{NA^*}$  were obtained.

As the experimental execution of the experiments grants the irradiation is turned on or off between the beam intensity of 0 [nA] and  $I$  [nA], where  $I$  is always constant for the measurement dataset, the generated radionuclides can be compared to a step input of a radiotracer (see chapter 4.2.1.3). This fact allows for fitting the experimental data with a sigmoidal function (S-curve). In this case, the Boltzmann function (4) from the Origin 2017 (OriginLab, USA) software was used.

$$y = A_2 + \frac{A_1 - A_2}{1 + e^{(x-x_0)/dx}} \quad (4)$$

where  $A_1$  is the initial value,  $A_2$  is the final value,  $x_0$  is the inflexion point and  $dx$  is the slope.

By plotting the  $NA^*$  as a function of time and using a Boltzmann fit, the maximum of the signal corresponding to the stationary state (upper boundary of the S-curve is either parameter  $A_1$  or  $A_2$  depending on the initial state), here denoted as a parameter  $A$  and its error  $\sigma_A$  were obtained. Consequently, the normalized yield  $\alpha$  and its error  $\sigma_\alpha$  were calculated by using the formula (5) and (6) respectively.

$$\alpha = \frac{NA^*}{A} \quad (5)$$

$$\sigma_\alpha = \sqrt{\left(\frac{\sigma_{NA^*}}{A}\right)^2 + \left(\frac{-NA^* \cdot \sigma_A}{A^2}\right)^2} \quad (6)$$

This allowed for constructing a normalized yield dependency on time. The normalized parameter  $\alpha$  basically represents the percentage of stationary state, that was reached at any given time.

In the figures 28 and 39, empty points denote datapoints laying below the baseline, which is physically impossible, and thus these values were substituted by the value of  $\alpha = 0$ .

### 6.2 Comparison of flow rates

During the experiment in November 2022, the glass mixing chamber (see section 5.4.1) was used. As previously mentioned, this glass mixing chamber was originally developed for mixing of liquids and mechanically measuring their flow rate. Thus, it has relatively big mixing volume and all in all non-ideal geometry for this application, which causes longer delivery times from the source to the PILS impactor chamber.

In figure 28, Screen OFF state indicates the screen (see section 5.2) was lifted during the measurement and the accelerated beam started interacting with the target foil. However, there is a slight delay between the start of the measurement and the screen being lifted. This delay was measured and calculated as  $1.84 \pm 0.09$  s. The transport by the capillary to the mixing chamber takes 2.0 s (for GJT flow  $1.5 \text{ L min}^{-1}$ ) (Bartl, Běhal, Matlocha *et al.*, 2023). As shown in the figure 28, which depicts the data

from November 2022, the influx of the detected EVRs is slow, with mean transport time of  $9.27 \pm 0.35$  s. The flush was, however, much faster; it took only  $4.73 \pm 0.45$  s. However, the beam intensity was overall lower during the November 2022 experiment, leading to lower count rates. This projects to the data by higher scatter. Thus, the flush time may be affected by lower statistical accuracy. In addition, the glass mixing chamber was used in this experiment, which was clearly far from ideal and caused the radionuclides to be somewhat slower when the beam was turned ON.

When the transport time through capillary (2.0 s) and the screen lifting delay ( $1.84 \pm 0.09$  s) are subtracted from the mean transport time, the mean transport time through the glass mixing chamber and the PILS is 5.43 s.

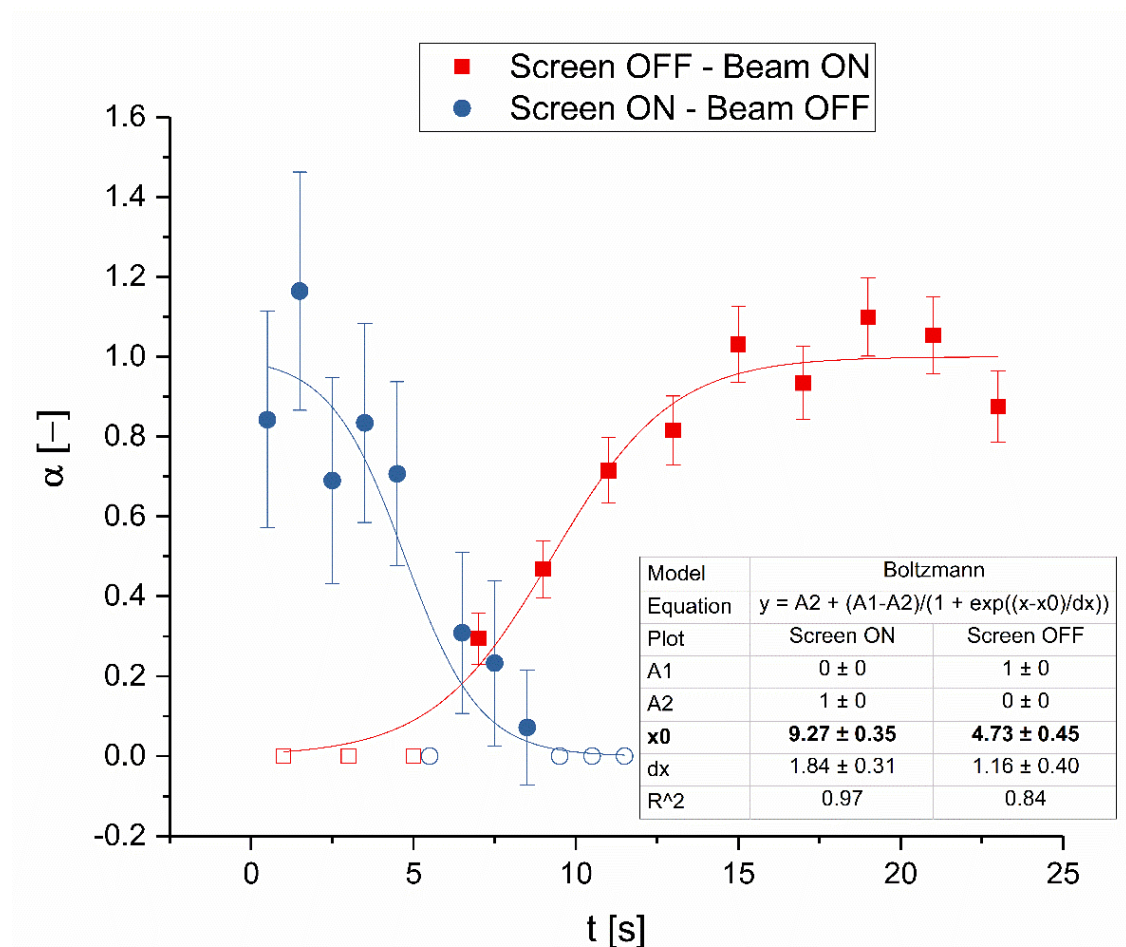


Figure 28: November 2022 experiment with the glass mixing chamber.

In April 2023 experiment, the glass mixing chamber was exchanged with the gas mixer (see section 5.4.2). The gas mixer is, in contrast with the glass mixing chamber, made for mixing gasses and has very low inner volume. It is also equipped with a check valve to prevent the air to going back into the GJT system.

In figure 29, a distinct symmetry of the curves can be seen, which suggests correct operation. The influx and flush mean transport times have much closer values than in the case of the experiment in November 2022. The slow influx in November 2022 can be explained by the big volume of the glass mixing chamber and, in addition, possibly non-ideal shape for mixing gasses, causing unwanted turbulences and thus delay. In case of the April 2023 influx experiments,  $7.51 \pm 0.35$  s mean transport

time was achieved leading to significant improvement with difference of approx. 1.7 s compared to the November 2022 experiment. The mean flush time was  $6.54 \pm 0.11$  s.

Same as in November 2022, there is also the same delay ( $1.84 \pm 0.09$  s) in the April 2023 experiment caused by lifting the screen. The GJT system flow was again set to  $1.5 \text{ L min}^{-1}$  leading to the transport time of 2.0 s through the capillary to the PILS.

When the transport time through capillary (2.0 s) and the screen lifting delay ( $1.84 \pm 0.09$  s) are subtracted from the mean transport time, the mean transport time through the gas mixer and the PILS is only 3.67 s.

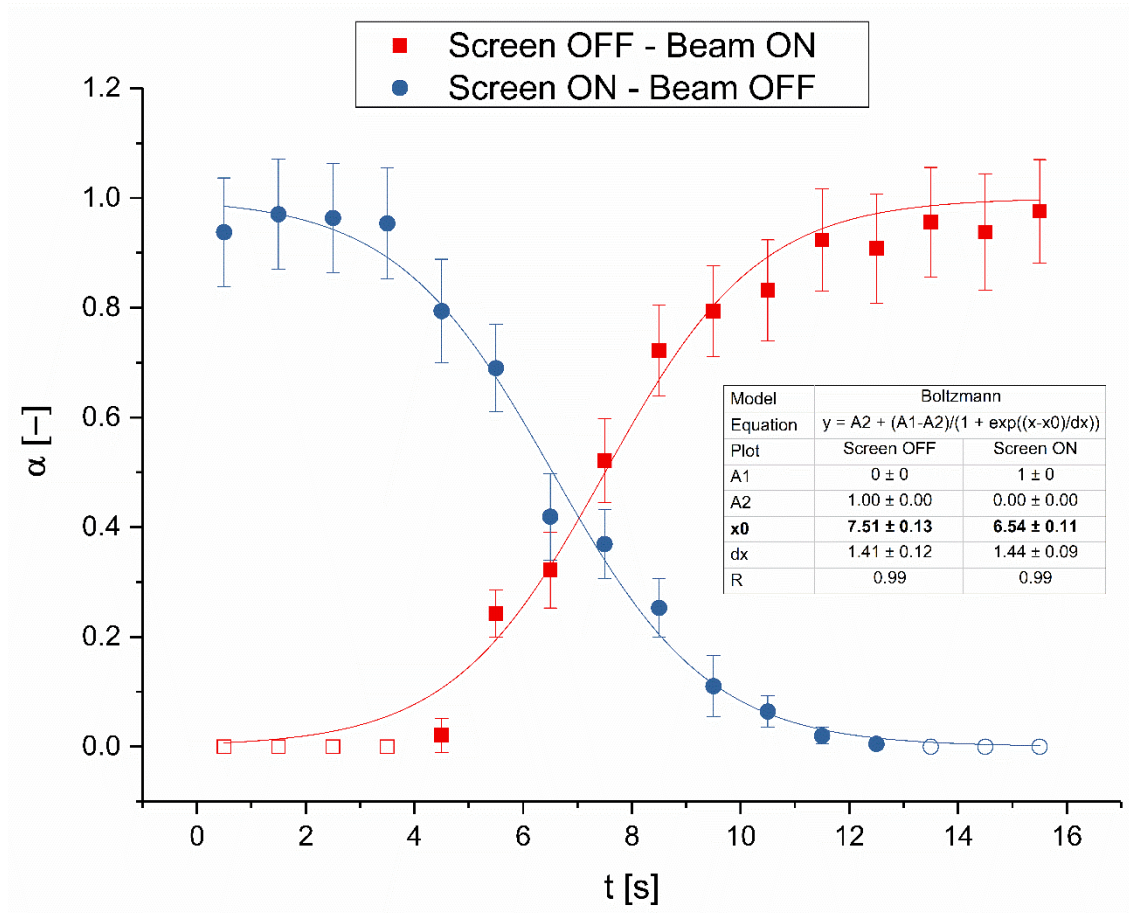


Figure 29: April 2023 experiment with the gas mixer.

## Conclusion

The theoretical part of this thesis covered the properties and preparation of transactinides. It also discussed the use of chemical homologues in transactinide research, with the emphasis on thallium as a Nh homologue. Various approaches to the problematics of detection and extraction of transactinides in the liquid phase were researched and experimental apparatuses used in this research topic worldwide were discussed in detail.

In experimental part of this thesis, two different mixing chambers were tested as an entry point for a state-of-the-art gas-into-liquid aerosol dissolution system (called the PILS). The November 2022 experiment was carried out using an old glass mixing chamber, which was originally designed for liquids. The glass mixing chamber showed that its properties for this application were far from ideal, e.g., too large mixing volume with unnecessarily complicated geometry. These drawbacks led to extended mean transport time. The influx mean transport time was measured as  $9.27 \pm 0.35$  s. The flush out mean transport time was determined as  $4.73 \pm 0.45$  s. Furthermore, the beam intensity was overall lower during the November 2022 experiment, which lead to lower count rates. This reflected in the data by higher scatter. Thus, the flush out time was probably affected by lower statistical accuracy. Graphic illustration of the data is displayed in the figure 28.

The April 2023 experiment used the gas mixer from Bronckhorst, which was specifically designed for mixing two gases. In this experiment, significant improvement in mean transport times was shown. The influx mean transport time was measured as  $7.51 \pm 0.35$  s, which is approx. 1.7 s faster compared to the November 2022 time. The flush out transport time was  $6.54 \pm 0.11$  s (slightly longer time but with much reliable data). The symmetry of the curves in the figure 29 suggests the correct operation of the gas mixer.

Both experiments showed a delay of  $1.84 \pm 0.09$  s caused by time gap between the start of the measurement and lifting the screen. Another delay of 2.0 s is caused by the transport of the EVRs via the GJT system to the mixing chamber. By subtracting these values from the measured mean transport times, mean transport times through the mixing chambers and the PILS were obtained as 5.43 s for glass mixing chamber and 3.67 s for the gas mixer.

Overall, it was achieved significant improvement in the mean transport times by exchanging the mixing chamber. The obtained knowledge will lead to better understanding the transport dynamics and contribute to the optimalization of the experimental parameters and to overall improvement of the experimental system.

## 7 References

Aronsson, P.O. *et al.* (1974). SISAK—A new technique for rapid, continuous (radio)chemical separations. *J Inorg Nucl Chem*, vol.36, no. 11, p. 2397-2403.

[www.doi.org/10.1016/0022-1902\(74\)80446-X](http://www.doi.org/10.1016/0022-1902(74)80446-X)

Bartl, P. (2022). Dissertation on Study of Extraction of Transactinide Homologues. CTU in Prague.

Bartl, P., Běhal, R., Matlocha, T. *et al.* (2023). MARGE – New modular robotic gas-jet target system for the chemistry of SHE homologues studies. *Nucl Instrum Methods Phys Res A*, vol. 1052.

[www.doi.org/10.1016/j.nima.2023.168280](http://www.doi.org/10.1016/j.nima.2023.168280)

Bartl, P., Němec, M., Zach, V. *et al.* (2023). Fast on-line dissolution of KCl aerosol particulates for liquid-phase chemistry with homologues of superheavy elements. *Nucl Instrum Methods Phys Res A*, vol. 1055.

[www.doi.org/10.1016/j.nima.2023.168500](http://www.doi.org/10.1016/j.nima.2023.168500)

Conesa, J.A. (2019). *Chemical Reactor Design: Mathematical Modeling and Applications*. p. 3-7.

[www.doi.org/10.1002/9783527823376](http://www.doi.org/10.1002/9783527823376)

De Felice, P. *et al.* (2017). Practical implementation of ISO 11929: 2010. *Appl Radiat Isot*, vol.126, p. 256-262.

[www.doi.org/10.1016/j.apradiso.2017.02.004](http://www.doi.org/10.1016/j.apradiso.2017.02.004)

Eibach, M. *et al.* (2010). Transport of fission products with a helium gas-jet at TRIGA-SPEC. *Nucl Instrum Methods Phys Res A*, vol. 613, no. 2, p. 226-231.

[www.doi.org/10.1016/j.nima.2009.11.034](http://www.doi.org/10.1016/j.nima.2009.11.034)

Even, J. *et al.* (2011). The recoil transfer chamber – An interface to connect the physical preseparator TASCA with chemistry and counting setups. *Nucl Instrum Methods Phys Res A*, vol. 638, no. 1, p. 157-164.

[www.doi.org/10.1016/j.nima.2011.02.053](http://www.doi.org/10.1016/j.nima.2011.02.053)

Greenwood, N.N., Earnshaw, A. (1997). Chemistry of the Elements. p. 216-241.

[www.doi.org/10.1016/B978-0-7506-3365-9.50013-4](http://www.doi.org/10.1016/B978-0-7506-3365-9.50013-4)

Hagino, K. (2019). Superheavy Elements: Beyond the 7th Period in the Periodic Table. AAPPS Bulletin, vol. 29, no. 1, p. 31-37.

[www.doi.org/10.48550/arXiv.1812.05805](http://www.doi.org/10.48550/arXiv.1812.05805)

Hofmann, S. *et al.* (2018). On the discovery of new elements (IUPAC/IUPAP Provisional Report). Pure and Applied Chemistry, vol. 90, no. 11, p. 1773-1832.

[www.doi.org/10.1515/pac-2018-0918](http://www.doi.org/10.1515/pac-2018-0918)

Ichimiya, T., Narita, T., Kitao, K. (1998). Natural background Gamma-ray spectrum; List of Gamma-rays ordered in energy from natural radionuclides.

[www.doi.org/10.11484/jaeri-data-code-98-008](http://www.doi.org/10.11484/jaeri-data-code-98-008)

Kaji, D. *et al.* (2013). Gas-filled recoil ion separator GARIS-II. Nucl Instrum Methods Phys Res B, vol. 317, p. 311-314.

[www.doi.org/10.1016/j.nimb.2013.05.085](http://www.doi.org/10.1016/j.nimb.2013.05.085)

Kaji, D., Morita, K., Morimoto, K. *et al.* (2003). Status of heavy element synthesis in RIKEN. Journal of Radioanalytical and Nuclear Chemistry, vol. 255, p. 77–80.

[www.doi.org/10.1023/A:1022223613289](http://www.doi.org/10.1023/A:1022223613289)

Karol, P.J. *et al.* (2016). Discovery of the elements with atomic numbers  $Z = 113, 115$  and  $117$  (IUPAC Technical Report). Pure and Applied Chemistry, vol. 88, no. 1-2, p. 139-153.

[www.doi.org/10.1515/pac-2015-0502](http://www.doi.org/10.1515/pac-2015-0502)

Morita, K. (2015). SHE research at RIKEN/GARIS. Nuclear Physics A, vol. 944, p. 30-61.

[www.doi.org/10.1016/j.nuclphysa.2015.10.007](http://www.doi.org/10.1016/j.nuclphysa.2015.10.007)

Nagame, Y. *et al.* (2003). Transactinide nuclear chemistry at JAERI. Czechoslovak Journal of Physics, vol. 53, p. A299-A304.

[www.doi.org/10.1007/s10582-003-0038-3](http://www.doi.org/10.1007/s10582-003-0038-3)

Nagame, Y. *et al.* (2005). Chemical studies on rutherfordium (Rf) at JAERI. Radiochimica Acta, vol. 93, p. 519-526.

[www.doi.org/10.1524/ract.2005.93.9-10.519](http://www.doi.org/10.1524/ract.2005.93.9-10.519)

Němec, M., Čubová, K., Semelová, M., Bartl, P. (2020). Praktikum z jaderné chemie a radiochemie I. Česká technika. ISBN: 978-80-01-06688-1

Oganessian, Yu.Ts., Rykaczewski, K.P. (2015). A beachhead on the island of stability. Physics Today, vol. 68, no. 8, p. 32-38.

[www.doi.org/10.1063/PT.3.2880](http://www.doi.org/10.1063/PT.3.2880)

Oganessian, Yu.Ts., Utyonkov, V.K., Popeko A.G. *et al.* (2022). DGFRS-2—A gas-filled recoil separator for the Dubna Super Heavy Element Factory. Nucl Instrum Methods Phys Res A, vol. 1033.

[www.doi.org/10.1016/j.nima.2022.166640](http://www.doi.org/10.1016/j.nima.2022.166640)

Ooe, K. *et al.* (2015). Development of a new continuous dissolution apparatus with a hydrophobic membrane for superheavy element chemistry. J Radioanal Nucl Chem, vol. 303, p. 1317–1320

[www.doi.org/10.1007/s10967-014-3469-3](http://www.doi.org/10.1007/s10967-014-3469-3)

Omtvedt, J.P. *et al.* (1998). Review of the SISAK system in transactinide research: recent developments and future prospects. J Alloys Compd, p. 271-273, p. 303-306.

[www.doi.org/10.1016/S0925-8388\(98\)00076-0](http://www.doi.org/10.1016/S0925-8388(98)00076-0)

Rowe, M.W. *et al.* (2000). Recent studies of proton drip-line nuclei using the Berkeley Gas-filled Separator. AIP Conference Proceedings, vol. 518, no. 1, p. 95–104.

[www.doi.org/10.1063/1.1306003](http://www.doi.org/10.1063/1.1306003)

Semchenkov, A. *et al.* (2008). The TransActinide Separator and Chemistry Apparatus (TASCA) at GSI – Optimization of ion-optical structures and magnet designs. *Nucl Instrum Methods Phys Res B*, vol. 266, no. 19-20, p. 4153-4161.

[www.doi.org/10.1016/j.nimb.2008.05.132](http://www.doi.org/10.1016/j.nimb.2008.05.132)

Schädel, M. *et al.* (1988). Fast radiochemical separations with an automated rapid chemistry apparatus. *Nucl Instrum Methods Phys Res A*, vol. 264, no. 2-3, p. 308-318.

[www.doi.org/10.1016/0168-9002\(88\)90920-5](http://www.doi.org/10.1016/0168-9002(88)90920-5)

Schädel, M. *et al.* (1989). ARCA II – A New Apparatus for Fast, Repetitive HPLC Separations. *Radiochim Acta*, vol. 48, p. 171-176.

[www.doi.org/10.1524/ract.1989.48.34.171](http://www.doi.org/10.1524/ract.1989.48.34.171)

Schwerdtfeger, P., Smits, O., Pyykkö, P. (2020). The periodic table and the physics that drives it. *Nature Reviews Chemistry*, vol. 4, no. 7, p. 359-380.

[www.doi.org/10.1038/s41570-020-0195-y](http://www.doi.org/10.1038/s41570-020-0195-y)

Silva, R. J. *et al.* (1977). A gas-jet recoil-transport system for fission products and its application to a continuous chemical separation procedure in the gas phase. *Nucl Instrum Methods*, vol. 147, no. 2, p. 371-378.

[www.doi.org/10.1016/0029-554X\(77\)90272-5](http://www.doi.org/10.1016/0029-554X(77)90272-5)

Subotic, K. *et al.* (2002). Evaporation residue collection efficiencies and position spectra of the Dubna gas-filled recoil separator. *Nucl Instrum Methods Phys Res A*, vol. 481, no. 1-3, p. 71-80.

[www.doi.org/10.1016/S0168-9002\(01\)01367-5](http://www.doi.org/10.1016/S0168-9002(01)01367-5)

Thompson, S.G., Tsang, C.F. (1972). Superheavy elements. *Science*, vol. 178, no. 4065, p. 1047-1055.

[www.doi.org/10.1126/science.178.4065.1047](http://www.doi.org/10.1126/science.178.4065.1047)

Tiebel, G. Dutheil, P., Dressler, R. *et al.* (2022). The SINQ gas-jet facility as a source for radionuclides from neutron-induced fission of <sup>235</sup>U. *Nucl Instrum Methods Phys Res A*, vol. 1041.

[www.doi.org/10.1016/j.nima.2022.167360](http://www.doi.org/10.1016/j.nima.2022.167360)



Terranova, M.L., Tavares, O.A.P. (2022). The periodic table of the elements: the search for transactinides and beyond. *Rendiconti Lincei. Scienze Fisiche e Naturali*, no. 33, p. 1-16.

[www.doi.org/10.1007/s12210-022-01057-w](http://www.doi.org/10.1007/s12210-022-01057-w)

Türler, A. Gregorich, K.E. (2013). *Experimental Techniques*, p. 273. In: Schädel, M., Shaughnessy, D. (eds) *The Chemistry of Superheavy Elements*, p. 273. Springer Berlin, Heidelberg.

[www.doi.org/10.1007/978-3-642-37466-1](http://www.doi.org/10.1007/978-3-642-37466-1)

Wierczinski, B. *et al.* (1995). Fast On-line Solvent Extraction with the SISAK-3 Centrifuge System as a Test of Chemical Studies of the Elements 105 and 106. *Radiochimica Acta*, vol. 69, p. 77-80.

[www.doi.org/10.1524/ract.1995.69.2.77](http://www.doi.org/10.1524/ract.1995.69.2.77)

Weber, R. J. *et al.* (2001). A Particle-into-Liquid Collector for Rapid Measurement of Aerosol Bulk Chemical Composition. *Aerosol Sci Technol*, vol. 35, no. 3, p. 718-727.

[www.doi.org/10.1080/02786820152546761](http://www.doi.org/10.1080/02786820152546761)

Wolf, S.F. (2008). Trace Analysis of Actinides in Geological, Environmental, and Biological Matrices. In: Morss, L.R., Edelstein, N.M., Fuger, J. (eds) *The Chemistry of the Actinide and Transactinide Elements*. Springer, Dordrecht.

[www.doi.org/10.1007/1-4020-3598-5\\_30](http://www.doi.org/10.1007/1-4020-3598-5_30)

Wollnik, H. (1976). Principles behind a He-jet system and its application for isotope separation. *Nucl Instrum Methods*, vol. 139, p. 1-15.

[www.doi.org/10.1016/0029-554X\(76\)90691-1](http://www.doi.org/10.1016/0029-554X(76)90691-1)